Saturation of the polar cap potential: Inference from Alfvén wing arguments

Margaret G. Kivelson[1,2] and Aaron J. Ridley[3]

Received 26 January 2007; revised 23 October 2007; accepted 12 December 2007; published 17 May 2008.

[1] The cross polar cap potential varies roughly linearly with the solar wind electric field for nominal conditions but asymptotes to a constant value of order 200 kV for large electric field. When the impedance of the solar wind across open polar cap field lines dominates the impedance of the ionosphere, Alfvén waves incident from the solar wind are partially reflected, reducing the signal in the polar cap. Thus, the ratio of the cross polar cap potential to the potential imposed by the solar wind is $2\Sigma_A/(\Sigma_P + \Sigma_A)$, where Σ_A is the Alfvén conductance of the solar wind ($= (\rho_{sw}/\mu_o)^{1/2}/B_{sw}$) to within a density-dependent factor on average of order 1, Σ_P is the Pedersen conductance of the ionosphere, and ρ_{sw} (B_{sw}) is the density (magnetic field magnitude) of the solar wind. For small B_{sw}, the response is proportional to B_{sw}. For large B_{sw}, the cross polar cap potential depends only on the solar wind dynamic pressure (with small viscous and density-dependent corrections). Quantitative estimates require knowledge of Σ_P and the dependence of the potential imposed by the solar wind on its measured properties; standard assumptions yield saturation levels consistent with observations made during 13 storm intervals. Previous explanations of saturation have invoked changing reconnection efficiency, specific characteristics of the Region 1 current system, or the effect of the bow shock on the reconnecting plasma. Although our relation is mathematically similar to some previously proposed, our arguments place no constraints on reconnection efficiency or on magnetospheric geometry.

Citation: Kivelson, M. G., and A. J. Ridley (2008), Saturation of the polar cap potential: Inference from Alfvén wing arguments, *J. Geophys. Res.*, *113*, A05214, doi:10.1029/2007JA012302.

1. Introduction

[2] Possibly as a result of a focus on space weather, recent years have witnessed an increased interest in understanding the response of the magnetosphere to extreme conditions in the solar wind [see, e.g., *Richardson et al.*, 2006]. Many activity-related parameters within the magnetosphere are found to increase as functions of solar wind parameters, such as the dynamic pressure, the southward component of the magnetic field, and the solar wind electric field (E_{sw}). Some of the earliest models of the ionospheric electric potential pattern used ground-based magnetic perturbations linearly related to the interplanetary magnetic field B_y and B_z components to describe the potential pattern for any IMF orientation [*Friis-Christensen et al.*, 1985; *Papitashvili et al.*, 1994; *Ridley et al.*, 2000]. Other studies [e.g., *Weimer*, 1996; *Boyle et al.*, 1997] also identified an approximately linear relationship of the electric potential to the IMF. None of these studies included large-amplitude IMF values and consequently did not reveal the saturation that had been reported earlier. For example, *Weimer et al.* [1990] and *Reiff et al.* [1981] found that the auroral electrojet (*AE*) index and the cross polar cap potential (CPCP) saturates for large negative values of B_z. *Russell et al.* [2001] showed a number of time periods in which saturation may take place in the potential, although *Liemohn and Ridley* [2002] argued that those data could equally well be interpreted as linear responses. *Liemohn et al.* [2002] showed that a saturated field is needed during large storms to avoid significantly overdriving the inner magnetospheric dynamics, which would produce an unrealistically large value of *Dst*. *Hairston et al.* [2003, 2005] analyzed the CPCP during several superstorms in which E_{sw} attained values from 10 to 40 mV/m, far larger than the range available in earlier works. They demonstrated that the CPCP levels off at a value between 150 and 200 kV, with the critical electric field being less than 10 mV/m. Recently, *Ridley* [2005] identified 13 events in which clear saturation was observed in the ionospheric CPCP. They further showed that the saturation tended to occur when the solar wind Mach number decreased below approximately four (it is normally $\gtrsim 8$).

[1]Institute of Geophysics and Planetary Physics, UCLA, Los Angeles, California, USA.
[2]Department of Earth and Space Sciences, UCLA, Los Angeles, California, USA.
[3]Department of Atmospheres, Oceans, and Space Science, University of Michigan, Ann Arbor, Michigan, USA.

Copyright 2008 by the American Geophysical Union.
0148-0227/08/2007JA012302

[3] Various interpretations of the saturation phenomenon have been offered and are fully discussed by *Ridley* [2005] and by *Shepherd* [2007]. Here we summarize only a few of the key papers. The earliest discussion seems to be that of *Hill et al.* [1976] who addressed the role of ionospheric conductivity in controlling acceleration of magnetospheric particles at Mercury and Mars. They argued that the convection potential in a planetary magnetosphere can saturate either because the rate of magnetic merging at the magnetopause decreases for small magnetosheath Alfvén speed ($v_{A,sh}$) or because ionospheric currents become so large that there are "major alterations in the magnetic field near the dayside magnetopause." Both of these arguments imply that saturation occurs because reconnection efficiency changes in the limit of a large solar wind magnetic field. Hill *et al.* proposed a functional expression that incorporates both control parameters. They developed an order of magnitude equality that involves properties of the solar wind and the conductance of the ionosphere in the form

$$\Delta V = V_M/(1 + \Sigma_M/\Sigma_o) \tag{1}$$

where ΔV is the CPCP and $V_M = v_{A,Sh}B_M R_M$ is the maximum potential drop allowed by the merging process. Here $\Sigma_o = B_D/(B_M \mu_o v_{A,sh})$, B_M (B_D) is the magnetic field just outside of (inside of) the dayside magnetopause, R_M is the distance to the nose of the magnetosphere, $v_{A,Sh}$ is the Alfvén speed in the magnetosheath, and Σ_M is the effective ionospheric conductance. In a subsequent conference abstract, *Hill* [1984] suggested that the ionospheric control of the CPCP is related to the requirement that Region 1 currents close through the polar ionosphere.

[4] *Siscoe et al.* [2002a, hereinafter referred to as S2002a] tested the predictions of the *Hill et al.* [1976] model against results from a global magnetohydrodynamic (MHD) code in which saturation is observed. Citing *Hill et al.* [1976] and *Hill* [1984], they describe the Hill model as producing saturation through a nonlinear process in which the magnetic field arising from Region 1 currents weakens the internal field at the dayside reconnection site thereby limiting the speed at which reconnection occurs. The process is described through analysis of an equivalent circuit. For the purpose of comparing with the form that we develop later in this paper, we express the form given by Siscoe *et al.* in the notation of this paper as

$$\Delta V(\mathrm{kV}) = 57.6 E_{sw} p_{sw}^{1/3} F(\theta)/\left[p_{sw}^{1/2} + 0.0125 \xi \Sigma_o E_{sw} F(\theta)\right] \tag{2}$$

Here $E_{sw} = |\mathbf{u}_{sw} \times \mathbf{B}_{sw,yz}|$ is in mV/m, p_{sw} is the solar wind dynamic pressure in nPa, and $\xi\Sigma_o$ is the effective ionospheric conductance in S (Siemens) broken into a dimensionless factor (ξ, with values between 3 and 4) that depends on the geometry of the currents flowing in the ionosphere and another that represents the uniform ionospheric conductance (Σ_o). In the GSM coordinate system, $\mathbf{B}_{sw}$ is the interplanetary magnetic field in nT and $\mathbf{B}_{sw,yz} = \mathbf{B}_{sw} - \hat{\mathbf{x}}(\hat{\mathbf{x}} \cdot \mathbf{B}_{sw})$, $F(\theta)$ describes the reconnection efficiency in terms of the angle, θ, between $\mathbf{B}_{yz}$ and $\hat{\mathbf{z}}_{GSM}$ and $\mathbf{u}_{sw}$ is the solar wind velocity in km/s. A typical form used for $F(\theta)$ is $\sin^2(\theta/2)$. We have written equation (2) in terms of the contemporary dipole field strength although the S2002a expression allows for changes from the present value. Saturation sets in at high values of the electric field, asymptoting to

$$\Delta V_{\max}(\mathrm{kV}) = 4608 p_{sw}^{1/3}/\xi\Sigma_o \tag{3}$$

The numerical factors in equation (2) and (3) are based in part on first principles and in part on empirical relations.

[5] *Siscoe et al.* [2002a, 2002b] find that global MHD codes accord with the saturation predicted by their relationship. In their picture, solar wind ram pressure limits the current that flows in the Region 1 current system and this in turn limits the CPCP.

[6] From studies of the CPCP in another global MHD code, *Merkine et al.* [2003] concluded that the CPCP saturates as the solar wind electric field becomes large and that the saturation level is controlled by the ionospheric conductance. They argue that the geometry of the magnetopause is affected by the ionospheric conductance and provide a picture in which this change of geometry reduces the reconnection potential.

[7] *Ridley* [2007a] also utilizes an MHD model to attempt to describe the saturation of the potential. He shows that when the magnetic field becomes large, the Alfvénic Mach number becomes low. During these times, Alfven wings form on the magnetosphere, thereby shielding the solar wind electric field. He argues that this causes the saturation of the potential.

[8] In this paper, we expand upon the analysis of *Ridley* [2007a] to derive the dependence of the CPCP on solar wind and ionospheric properties. The underlying concept is that signals propagating into the ionosphere are partially reflected when the impedance of the source plasma differs from the impedance of the ionosphere and, in the limit, this reflection leads to the saturation observed. We focus on the arguments for this theoretical interpretation, introducing data principally to demonstrate that the predictions of the theory represent the behavior of the CPCP to lowest order. We postpone refinement of the quantitative predictions for later work.

2. Polar Cap Potential and Alfvén Wing Analysis

[9] As an introduction to our description of the physical mechanisms that result in the saturation of the CPCP, we consider the now standard description of the interaction of the flowing plasma of Jupiter's magnetosphere with the Galilean moons, treated as conducting bodies [*Southwood et al.*, 1980; *Neubauer*, 1980; *Kivelson et al.*, 2004]. In terms of $\mathbf{u}$, the flow speed of the ambient magnetospheric plasma in the rest frame of a moon, and $\mathbf{B_o}$, the ambient magnetospheric magnetic field, the upstream electric field is $\mathbf{E} = -\mathbf{u} \times \mathbf{B_o}$. In the simplest geometry, $\mathbf{u}$ and $\mathbf{B}_o$ are orthogonal and the potential drop across the diameter (D) of the moon is $V_o = uBD$. If the moon's Pedersen conductance (height-integrated Pedersen conductivity) is Σ_M, it is found that the potential drop across the moon is given by

$$\Delta V/V_o = 2\ \Sigma_A(\Sigma_M + 2\ \Sigma_A) \tag{4}$$

where $\Sigma_A = (\mu_o v_A)^{-1}$ is called the Alfvén conductance and $v_A = B/(\mu_o \rho)^{1/2}$ is the upstream Alfvén speed. A factor of 2

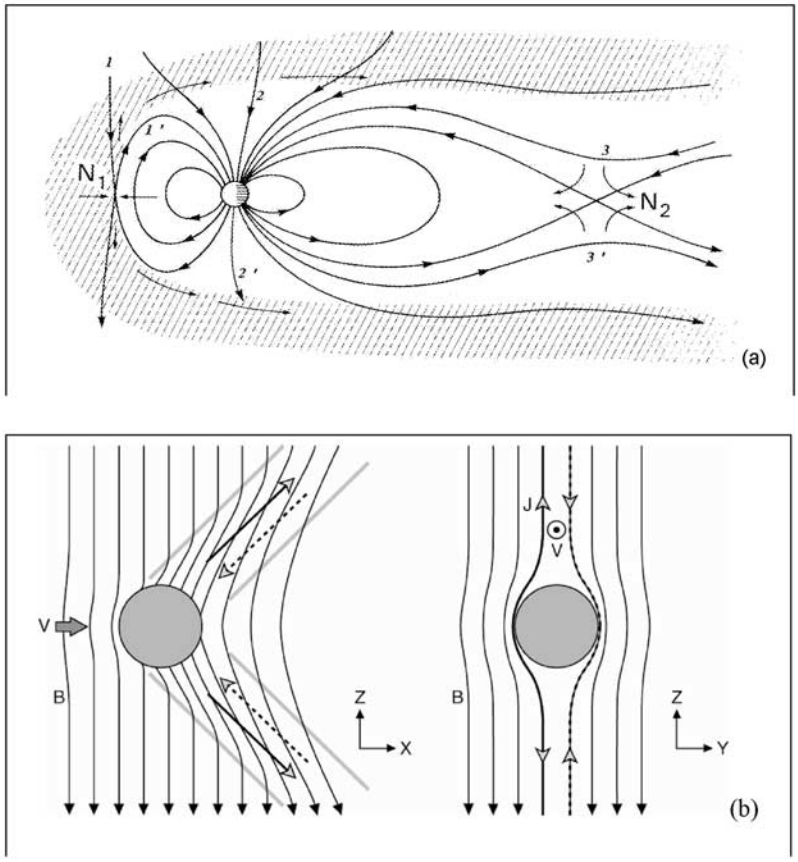

Figure 1. (a) Cross section of the magnetosphere projected into the noon-midnight plane (from Wikipedia version original by David Stern). Field lines are shown linking the polar cap with the solar wind. These open field lines carry field aligned currents into the polar ionosphere. (b) Schematic illustrations of the interaction of the Jovian plasma with the moon Io. To the left is a cut through the plane of the upstreamflow and field, equivalent to the noon-midnight meridian at Earth. To the right is a cut through the center of Io and perpendicular to the flow. This illustrates that some of the upstream plasma flows around Io and only a portion of the incident plasma actually encounters Io.

appears in the denominator of equation (4) because currents flow into the Galilean moons from both north and south and the total current closes through a region of net conductance Σ_M (Io and/or its ionosphere). Equation (4) is similar to the form applicable to a transmission line for which the impedance of the load does not match the impedance of the line. In this situation, the load reflects some part of the incident signal, which reduces the electric field imposed on it. The lower illustration of Figure 1 represents the interaction at Io. It shows (left) that flux tubes linking to Io are bent in the direction of the flow by field-aligned currents and (right) that only a fraction of the upstream plasma that would encounter Io in an unperturbed flow actually reaches it, implying that only a fraction of the potential drop across its diameter in the upstreamflow is actually imposed across the moon. Equation (4) indicates that the fraction is determined by the conductance of the moon and the Alfvén conductance of the plasma.

[10] Earth's magnetosphere, like the moons of Jupiter, is embedded in a flowing plasma: the solar wind. If reconnection has established a relatively steady open magnetospheric configuration, the linkage of solar wind flux tubes to the polar caps is analogous to the linkage of Jovian field lines to a Galilean moon. The analogy is illustrated by the upper portion of Figure 1, which shows field lines linking the polar cap to the solar wind. As at Io, the flowing plasma drags flux tubes across the obstacle and field-aligned currents carry Alfvénic perturbations from the flowing plasma into the conducting layers of the body. *Ridley* [2007a] used a formulation similar to that of equation (4) to describe the potential across the polar cap at Earth. His equations were based on the work of *Neubauer* [1980], which differs from that used here [*Southwood et al.*, 1980] only in the definition of Σ_A. Here we expand upon Ridley's work and modify his equations slightly as discussed below.

[11] In applying the concept of partial reflection to the polar cap, the analysis can be directly based on wave theory much as it is applied in the analysis of transmission lines. Because the field-aligned currents entering one polar cap at Earth are unlikely to cross the equator, we analyze each polar cap separately. The analysis makes use of the Pedersen conductance of the polar cap ionosphere, Σ_P. (Σ_P is the height-integrated Pedersen conductivity of the ionosphere. If I is the current in the direction of the electric field, E, in the ionosphere, then $\Sigma_P = I/E$ [see, e.g., *Mallinckrodt and Carlson*, 1978].) Hydromagnetic theory implies that a

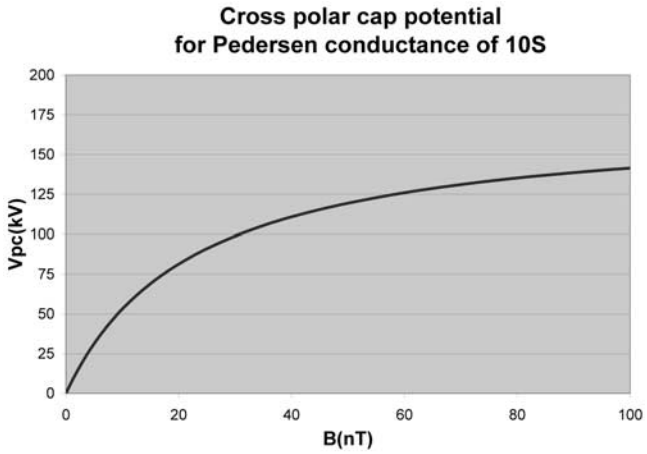

Figure 2. Cross polar-cap potential predicted by equation (8) versus B_{sw} for nominal values of ρ and u_{sw} and for Pedersen conductance = 10 S.

normally incident Alfvén wave encountering a change of impedance (Σ_A to Σ_P) in a length short compared with its wavelength is reflected with signal amplitude:

$$E_r = E_i\left(\Sigma_P^{-1} - \Sigma_A^{-1}\right)/\left(\Sigma_P^{-1} + \Sigma_A^{-1}\right) \tag{5}$$

When Σ_P is larger than Σ_A, the direction of the electric field in the reflected wave opposes that in the incoming wave, just as it does in the electromagnetic wave reflected from a mirrored surface. Continuity of the tangential electric field requires that the electric field transmitted be equal to the sum of the incident plus reflected fields:

$$E_t = E_i + E_r = 2E_i\Sigma_P^{-1}/\left(\Sigma_P^{-1} + \Sigma_A^{-1}\right) \tag{6}$$

If Σ_P is larger than Σ_A, the transmitted field is smaller than the incident field. From equation (6) (and ignoring convergence of field lines) the transmitted potential is

$$\Delta V_t = 2\Delta V_i\Sigma_A/(\Sigma_P + \Sigma_A) \tag{7}$$

[12] The denominators differ in equations (7) and (4) because of the decoupling of the two polar caps in the terrestrial case but the factor of 2 in the numerator remains so that when $\Sigma_P = \Sigma_A$ there is no reflection and $\Delta V_t = \Delta V_i$.

[13] Applying this form to the terrestrial case and initially neglecting the change of field and plasma properties between the solar wind and the ionosphere, we find that in each polar cap,

$$\Delta V = 2\,E_{sw}^R\,D\,\Sigma_A/(\Sigma_P + \Sigma_A) \tag{8}$$

where

$$E_{sw}^R = u_{sw}B_{sw,yz}\sin^2(\theta/2) \tag{9}$$

is the solar wind reconnection electric field and $B_{sw,yz}$ and θ are defined following equation (2). The dependence on θ is based on *Sonnerup* [1974] and *Kan and Lee* [1979]. D is defined as the distance across the unperturbed solar wind that contains field lines that reconnect as they encounter the dayside of the magnetosphere, $\Sigma_A = 1/(\mu_o v_A)$ is the Alfvén conductance of the solar wind and Σ_P is the Pedersen conductance of the ionosphere being considered.

[14] Although we have taken a fixed value for the ionospheric conductance, one expects that under most conditions the conductance of northern and southern ionospheres will differ and it is reasonable to imagine that the CPCPs will differ. However, some studies have shown that the potential does not vary significantly through the course of the year and that the auroral conductance may compensate for changes of the solar EUV-driven conductance [e.g., *Ridley*, 2007b].

[15] The form of equation (8) as a function of B_{sw} is plotted in Figure 2 for nominal values of the parameters (u_{sw} = 400 km/s, ρ_{sw} = 10 cm^{-3}, Σ_P = 10 S). At extremely large values of the IMF, the asymptote is ~170 kV. The form of equation (8) is similar (not identical) to that suggested for the polar cap potential at Earth by *Hill et al.* [1976] and S2002a. However, the present analysis rests on different arguments, appealing directly to the fact that a conducting obstacle (in this case, the magnetosphere) in a flowing plasma sets up Alfvénic perturbations that carry currents generated by the interaction.

[16] In obtaining equation (8), we neglected the possibility that the Alfvénic perturbations may be partially reflected where the open flux tubes cross the bow shock and the magnetopause. This neglect is justified. Most of the polar cap field lines cross the bow shock in regions where the shock is weak enough that the Alfvén speed changes only slightly across the surface and little reflection occurs. In the portion of the surface threaded by open field lines, the magnetopause is a rotational discontinuity across which the Alfvén speed does not change and there should be no reflected signal. Thus, the analysis that links the solar wind to the polar cap without consideration of intermediate boundaries is likely to be a good approximation.

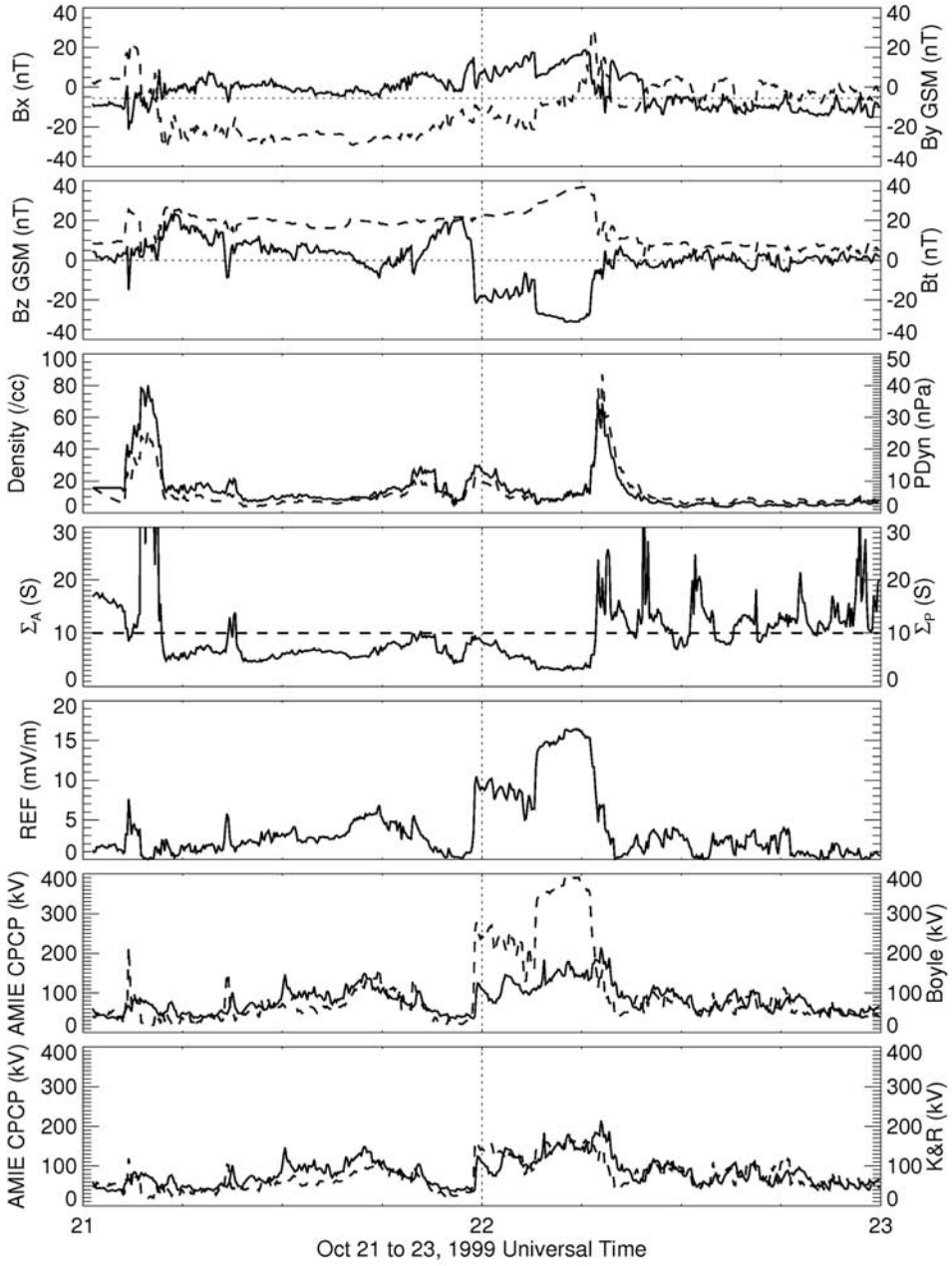

Figure 3a. A plot of solar wind properties and predictions of the polar cap potential for the intense storm interval of 21 to 23 October 1999. The top two panels provide information on the solar wind magnetic field GSM components and the field magnitude. The first (top) panel shows B_x (solid) and B_y (dashed). The second panel shows B_z (solid) and $|\mathbf{B}|$ (dashed). The third panel shows the density (solid lines, labels to the left) and the dynamic pressure (dashed lines, labels to the right), the fourth panel shows the Alfvén conductance of the solar wind in S and the assumed Pedersen conductance of the polar cap (solid dashed line at 10 S), the fifth panel shows the reconnection electric field, E_{rc} as defined in equation (9) in mV/m and the bottom two panel shows the cross polar cap potential in kV (solid lines). Dashed lines in the sixth panel are predictions of equation (14) from the work of *Boyle et al.* [1997]. Dashed lines in the seventh or bottom panel are the predictions of equation (13).

[17] Wave-based descriptions of momentum and energy coupling between the ionosphere and the magnetosphere [e.g., *Mallinckrodt and Carlson*, 1978] or magnetosheath [*Wright*, 1996] have been developed in the past. A wave framework avoids the inconsistencies that arise in relating fields and currents in different parts of the plasma through circuit analysis. When different parts of the plasma are in relative motion, there is no consistent definition of the electric field. The electric field defined in the rest frame of one part of the plasma differs from the electric field present in the rest frame of other parts of the plasma, and the circuit analysis approach that is often used for interpretation

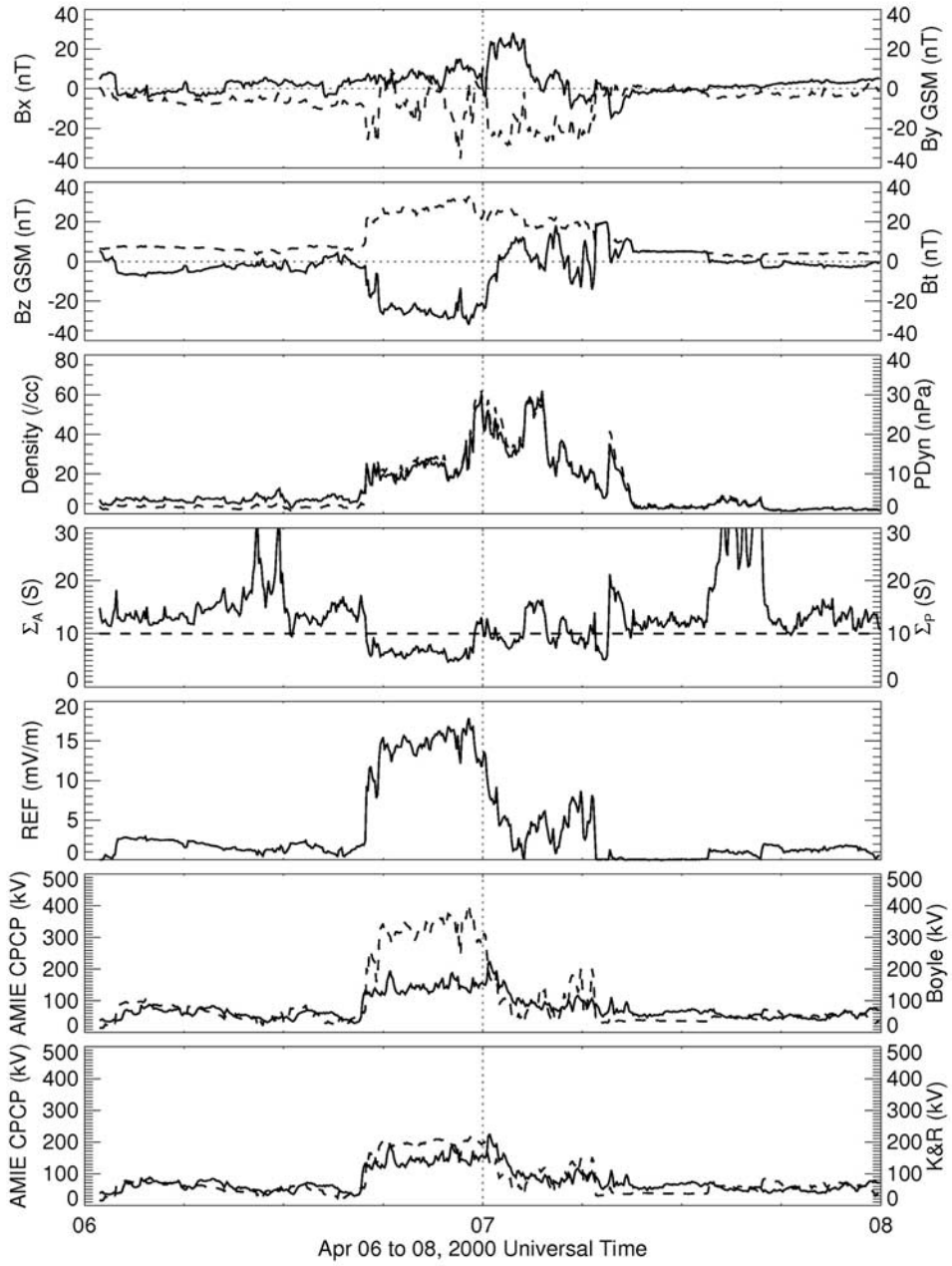

Figure 3b. As for Figure 3a but for the intense storm interval of 6 to 8 April 2000.

is flawed. This point has recently been elegantly elucidated by *Parker* [2007].

3. Use of Solar Wind Parameters in Calculation of Reflection at the Ionosphere

[18] The derivation of equation (8) assumes that the incoming wave at the top of the ionosphere can be characterized in terms of the solar wind electric field and the solar wind Alfvén conductance. Knowing that the Alfvén speed above the ionosphere is some 60 times larger than it is in the solar wind (and the Alfvén conductance is correspondingly some 60 times smaller), it is not unreasonable to question the use of solar wind wave properties. However, one can show that the changing conditions along the field line preserve the form applicable for uniform background conditions to within a correction factor. A derivation of the relation invokes the WKB method (http://farside.ph.utexas.edu/teaching/jk1/lectures/node70.html). Details are provided in Appendix A. The WKB analysis assumes that the length scale characteristic of changes of field and density along the flux tube linking the solar wind to the top of the ionosphere is long compared with the wavelength of the propagating wave. This condition is valid above the ionosphere except possibly across the magnetopause and the bow shock, whose effects on waves incident on the

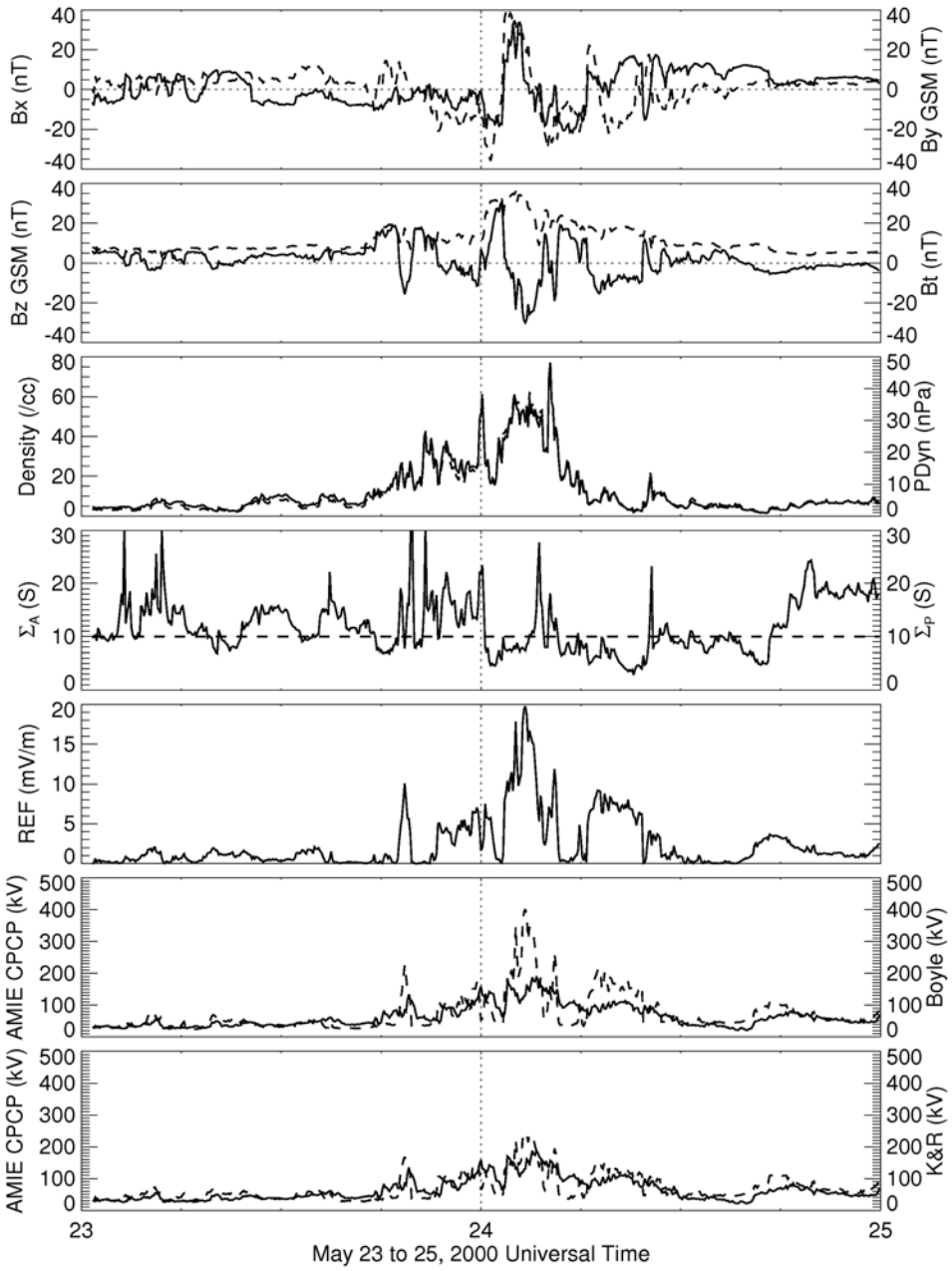

Figure 3c. As for Figure 3a but for the intense storm interval of 23 to 25 May 2000.

polar cap are small, as noted above. The ratio of $\Sigma_A E$ at a point s along the field line to its value in the solar wind is found to be $\kappa = [\rho(s)/\rho_{SW}]^{1/4}$. As discussed in the appendix, in the low altitude polar cap, the plasma density has been found to vary from slightly less than 1 cm^{-3} to ~100 cm^{-3} [*Chugunin et al.*, 2002; *Huddleston et al.*, 2005; *Laasko et al.*, 2002] and to depend on activity and illumination. Probable values of κ are likely to differ from 1 by no more than a factor of 2. As the densities in the low altitude polar cap are not routinely measured, we are forced to adopt a value of 1 with the understanding that this introduces errors of a few tens of percent in our predictions. If, however, data on the density above the ionosphere (ρ_{PC}) were to be available, a corrected form would replace $\Sigma_A = (\mu_o v_{A,SW})^{-1}$ by $\Sigma_A = (\rho_{pc}/\rho_{sw})^{1/4} (\mu_o v_{A,SW})^{-1}$ in equation (8).

4. Limiting Cases

[19] For nominal solar wind conditions at Earth, Σ_A exceeds Σ_P, or equivalently B_{sw} is less than $(\rho/\mu_o)^{1/2}/\Sigma_P$. In this case the CPCP is proportional to the solar wind electric field, increasing linearly with B_{sw}, and the full potential difference imposed on the polar cap is proportional to the potential drop across the portion of the

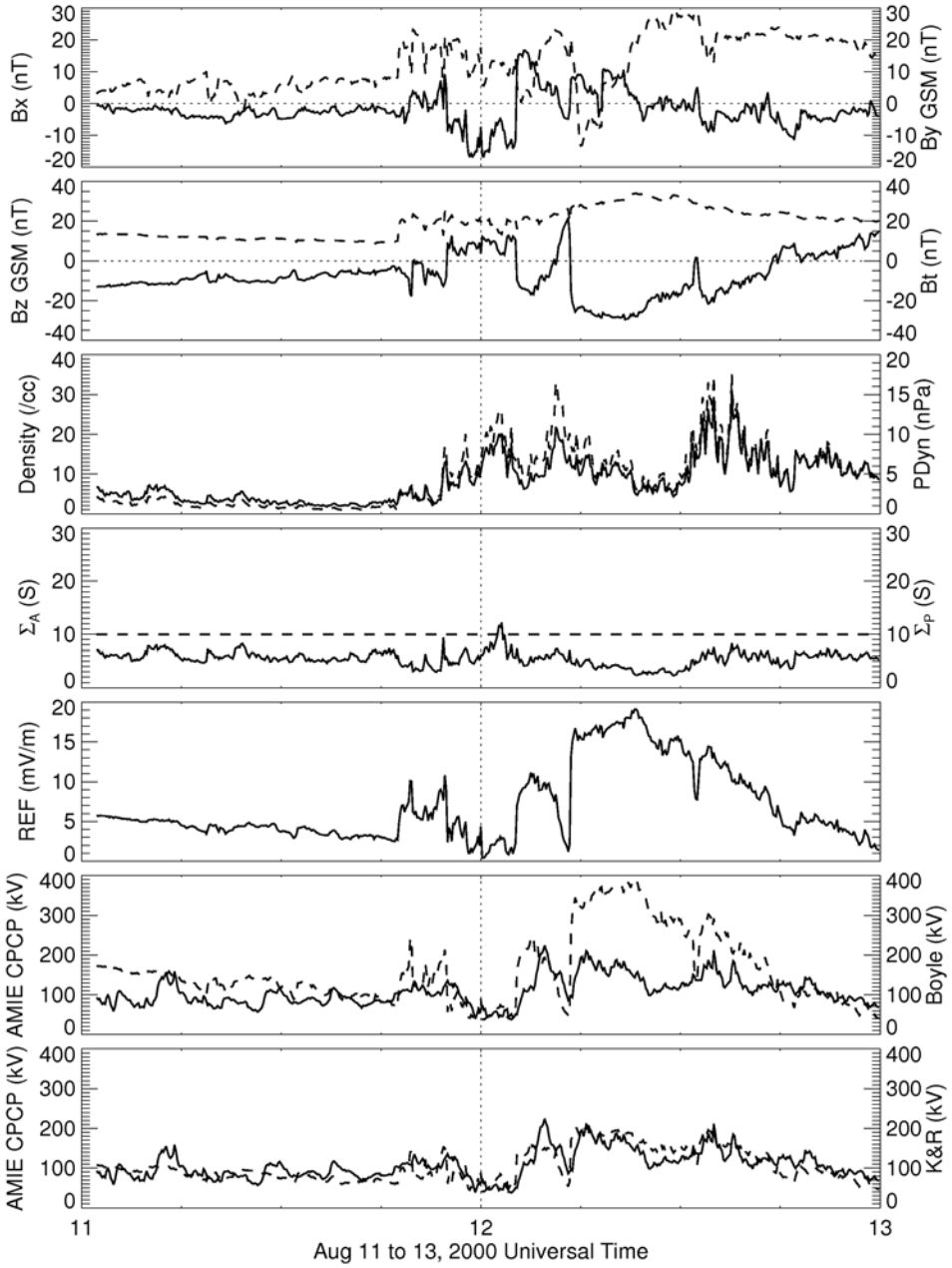

Figure 3d. As for Figure 3a but for the intense storm interval of 11 to 13 August 2000.

solar wind that has reconnected. In the opposite limit (large B_{sw}), equation (8) reduces to

$$\Delta V_{\max} \approx 2E^R_{sw} D\Sigma_A/\Sigma_P = 2D\left(\rho u^2_{sw}/\mu_o\right)^{1/2} \sin^2(\theta/2) \sin\lambda/\Sigma_P \tag{10}$$

Here λ is the cone angle of the IMF defined by $\sin\lambda = B_{sw,yz}/B_{sw}$ and the CPCP is independent of the magnitude of B_{sw} although it still depends on its orientation as well as the solar wind dynamic pressure, ρu^2_{sw}.

[20] Although the dependence on solar wind parameters is identical in equation (13) of S2002a and in our equation (10), the numerical values differ slightly. Comparing our CPCP for an assumed Σ_P = 10 S and the S2002a value using the effective Pedersen conductance of $\xi\Sigma$ = 21.7 S, the values differ by a factor of 1.77, with our prediction being smaller than that of S2002a. Setting our Σ_P to 21.7 S would increase the difference.

[21] One can estimate the critical value of the magnetic field at which the linear response rolls over for a nominal solar wind density of 10/cm^3 and an ionospheric conductance of roughly 10 S by setting $\Sigma_A = \Sigma_P$ in equation (8) to obtain

$$B_{crit} \approx (\rho/\mu_o)^{1/2}/\Sigma_P = 11.6 \text{ nT} \tag{11}$$

5. Comparison With Measurements

[22] We have used equation (8) (recognizing that it lacks a density-dependent factor $[\rho(s)/\rho_{SW}]^{1/4}$) to predict the polar

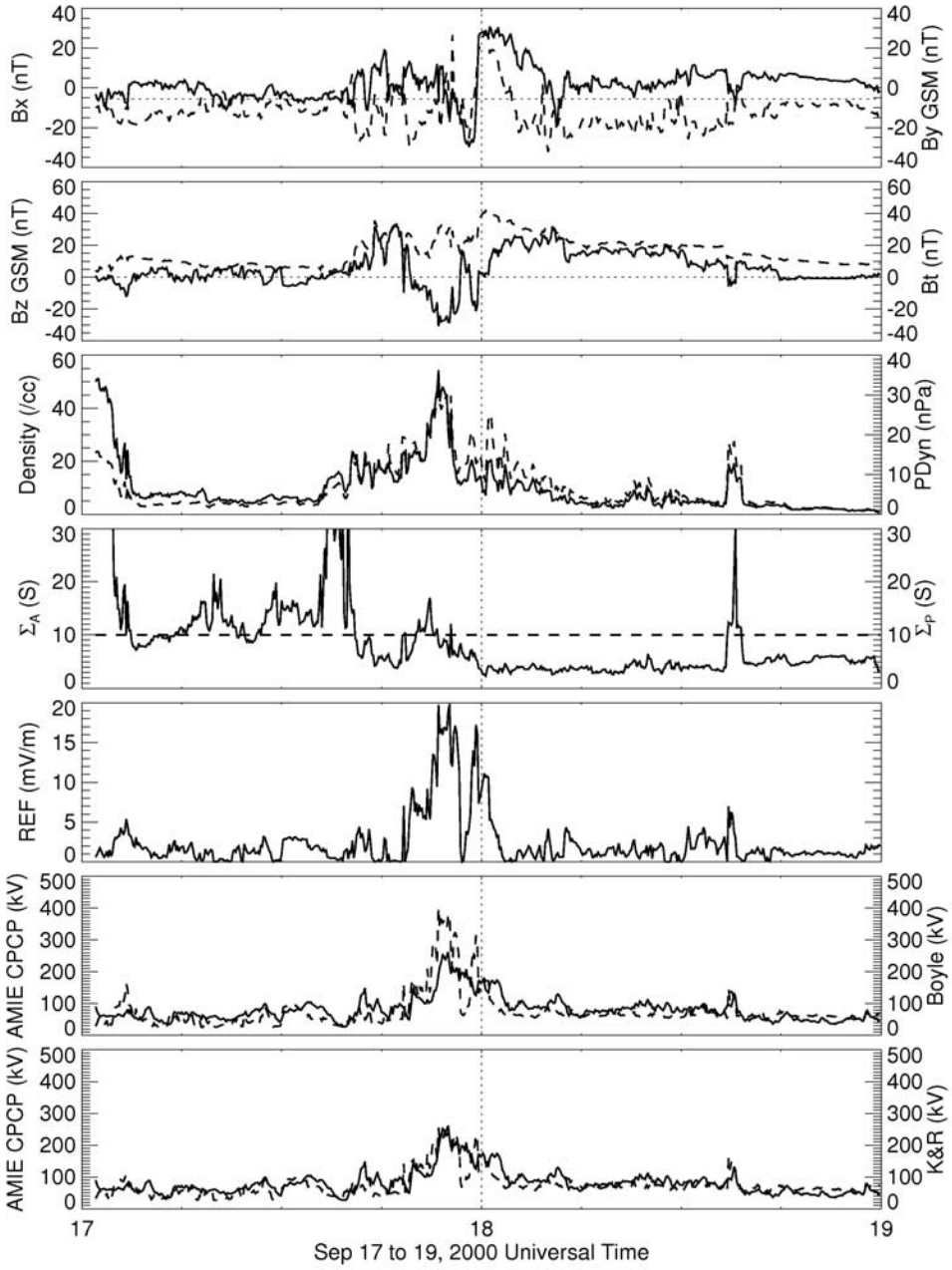

Figure 3e. As for Figure 3a but for the intense storm interval of 17 to 19 September 2000.

cap potential for the 13 storm intervals previously analyzed by *Ridley* [2005, Table 1]. The omission of the density-dependent factor, κ, introduces errors of tens of percent, and other sources of error are also present. Critical to testing the prediction is the approach used to establish the ''observed'' value. Various methods can be used to determine the ionospheric potential in the polar cap at auroral and subauroral latitudes. All are subject to uncertainties. For example, the CPCP can be estimated from in situ data provided by DMSP satellites flying across the polar convection zone. DMSP instruments measure the in situ cross-track velocity of the ions from which the electric field is inferred. However, if the satellite does not encounter the extrema of the potential pattern, the potential drop will be underestimated. Furthermore, the temporal cadence of such satellite measurements is the orbital period, of order 100 min, which is inadequate for the study of solar wind-driven variations. Changes during the tens of minutes needed to cross the polar cap cannot be resolved. As well, the spacecraft particle detectors are not dependable in low-density conditions, such as may exist on the nightside or during solar minimum.

[23] Radar techniques can also be used to establish the potential from convective flows. The SuperDARN network provides, in principle, near-global coverage of the ionospheric potential pattern, but the actual coverage depends on the backscatter intensity. When the activity level is either too low or too high, the scatter may not provide an accurate

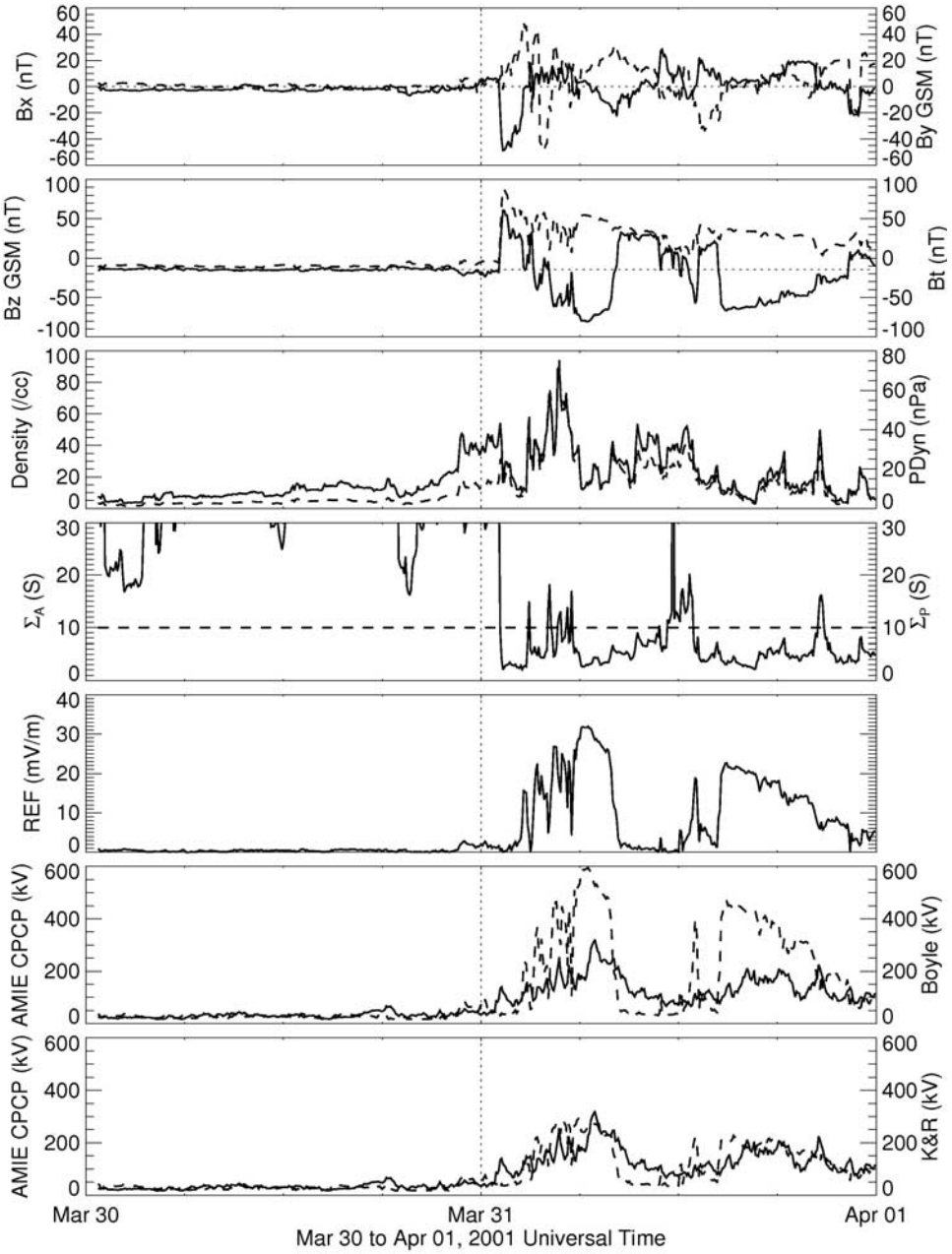

Figure 3f. As for Figure 3a but for the intense storm interval of 30 March to 1 April 2001.

determination of the flow velocities. In addition, the scattering amplitude may fluctuate dramatically and, consequently, the derived potential patterns may change markedly from time step to time step.

[24] A useful alternative technique is to infer the flow and ionospheric potential patterns from magnetic perturbations recorded on arrays of ground magnetometers using the assimilative mapping of ionospheric electrodynamics (AMIE) technique [*Richmond and Kamide*, 1988; *Ridley and Kihn*, 2004]. It is this technique that we have adopted to establish the ionospheric CPCPs that we compare with the predictions of equation (8). The potentials derived from the AMIE technique are themselves subject to uncertainties, especially because inversion of the magnetometer data makes use of poorly specified ionospheric conductance. However, studies have shown that the ionospheric potential is reasonably well specified using the AMIE approach. For example, *Kihn et al.* [2006] found good correspondence for a year's worth of DMSP-AMIE values that included some time intervals with large solar wind electric fields. *Bekerat et al.* [2005] compared AMIE estimates to those from measurements of DMSP for an entire year, including active time periods, and found good correspondence. No comparative studies of other global potential specification methods, such as SuperDARN, are available, so it is not known whether

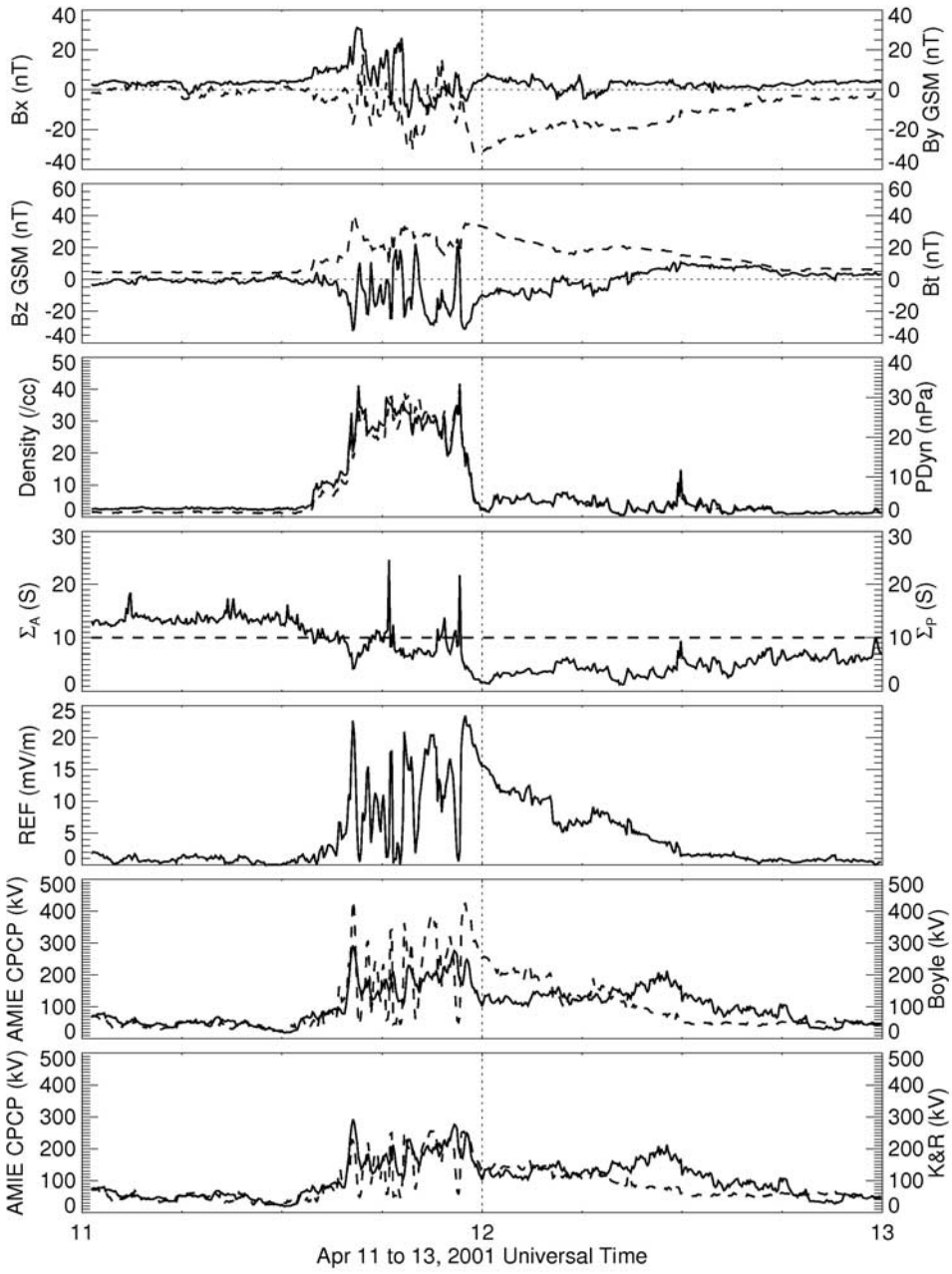

Figure 3g. As for Figure 3a but for the intense storm interval of 11 to 13 April 2001.

potential patterns inferred from such techniques are more accurate than those obtained from the AMIE technique. It should also be noted that both DMSP and SuperDARN show saturation of the CPCP, similar to that inferred by the AMIE technique using magnetometer data [*Shepherd et al.*, 2002; *Hairston et al.*, 2005].

[25] In the comparisons of data and the predictions of equation (8) that follow, both solar wind and AMIE data have been averaged to 5 min samples. The parameter D is taken as proportional to R_{mp} the distance to the nose of the magnetopause

$$D = 0.1\pi R_{mp} \tag{12}$$

Pressure balance is used to approximate R_{mp}/R_E as $[(2B_o)^2/2\mu_o p_{sw}]^{1/6}$. Here B_o is the equatorial surface field of Earth. The solar wind pressure is given by $p_{sw} = \rho u_{sw}^2 + B_{sw}^2/2\mu_o$, where the magnetic pressure is included because, in the storm-time events that we examine, it can become of order the dynamic pressure. (We do not include the thermal pressure of the solar wind because even during significant compression events, it generally remains small compared with the dynamic pressure.) As noted earlier, we set Σ_P to a nominal (fixed) value of 10 S, within a factor of $\sim$2 of values used elsewhere [e.g., *Siscoe et al.*, 2002a, 2002b]. Evidently, a value of conductance independent of geomagnetic conditions and

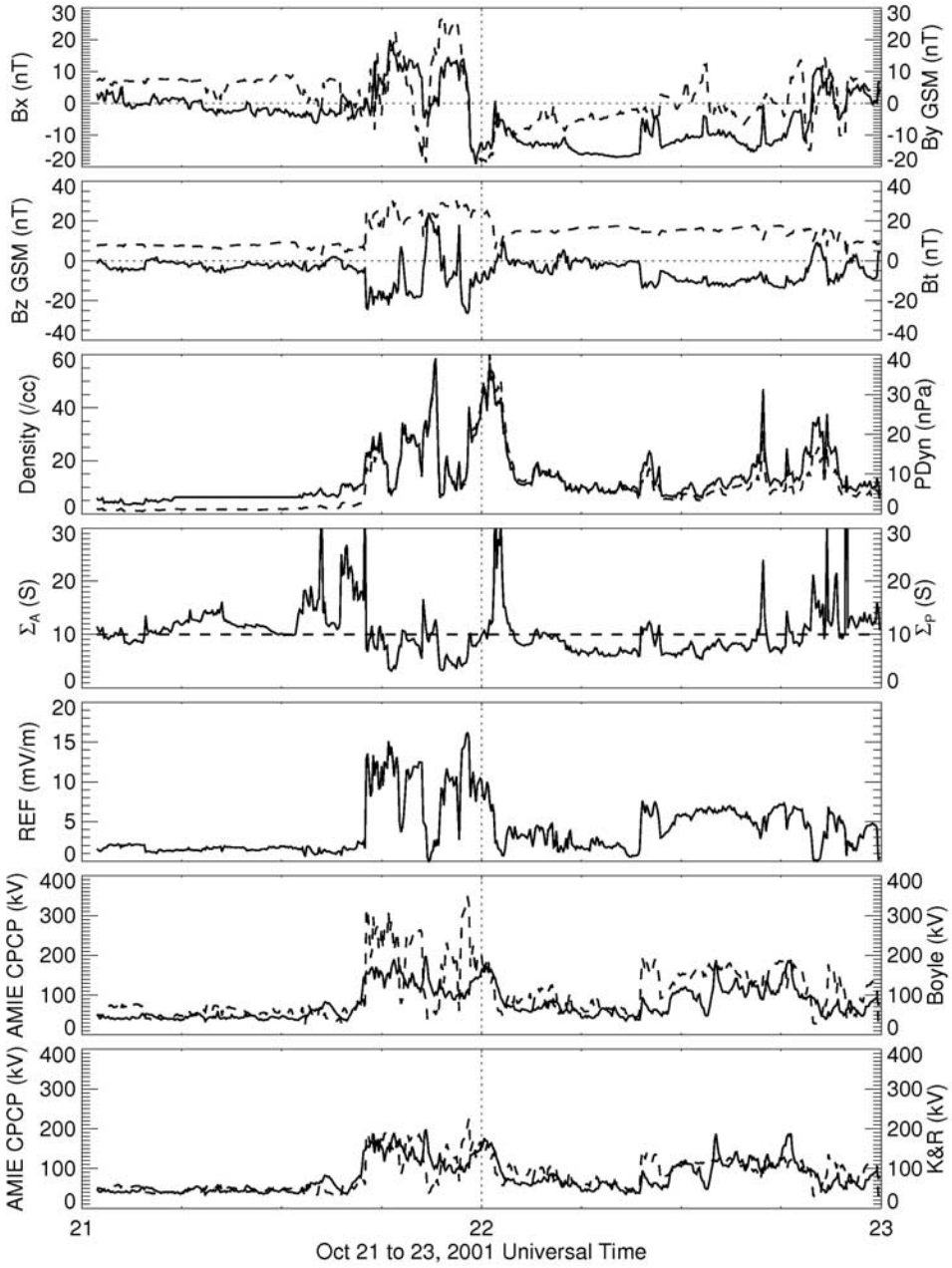

Figure 3h. As for Figure 3a but for the intense storm interval of 21 to 23 October 2001.

seasons is not plausible and the constant value assumed is an approximation. In addition, we have added a viscous interaction term identical to that used in the *Boyle et al.* [1997] study. Our final form for the total ionospheric CPCP (in standard SI units) is

$$V_{pc} = 10^{-7}u_x^2 + 0.2\pi B_{sw,yz}u_x \sin^2(\theta/2)R_{mp}\Sigma_A/(\Sigma_P + \Sigma_A) \quad (13)$$

Figures 3a–3h show the data (labeled by dates) for the 8 of 13 storms for which the hour-averaged reconnection electric field, E_{sw}^R, attained values greater than 15 mV/m at some time during a 2-days storm period. Properties of the solar wind needed to calculate the CPCP from equation (13) are plotted. The bottom panels of each plot show the CPCP obtained from the AMIE inversions (solid curves) and, superimposed as dashed curves, the predictions of a linear relation

$$V_{pc}(\mathrm{kV}) = 10^{-4}u_x(\mathrm{km/s})^2 + 11.7B_{sw}(\mathrm{nT})\sin^3(\theta/2) \quad (14)$$

from the work of *Boyle et al.* [1997] in the sixth panel and the predictions of equation (13) in the bottom panel. During intervals of large E_{sw}^R, equation (14) significantly overestimates the CPCP whereas equation (13) is quite successful in predicting its changing values. The predictions

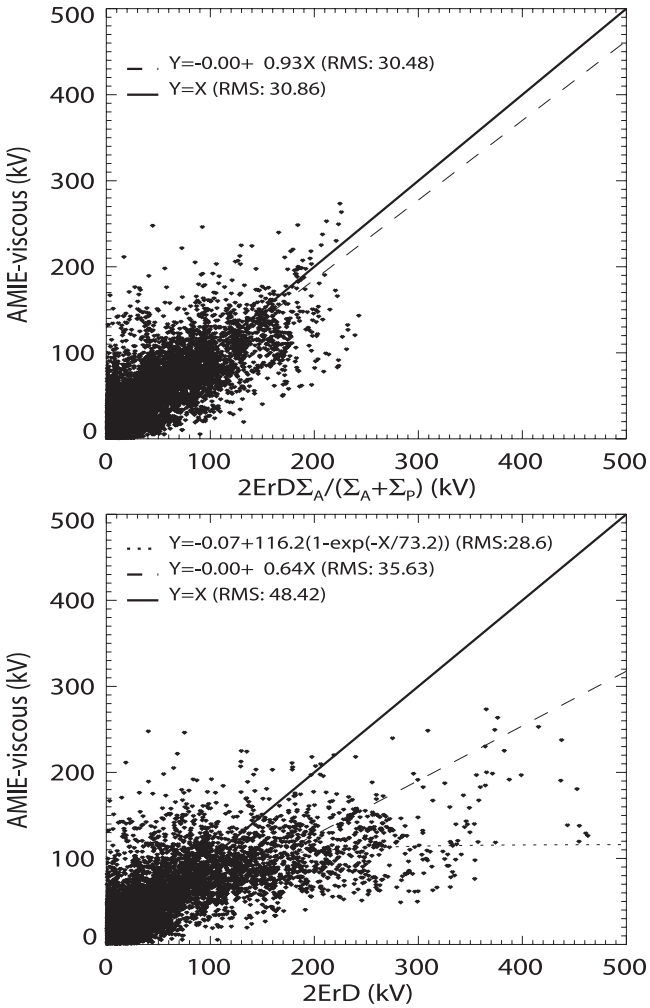

Figure 4a. a. Scatterplot for all data in 2-days intervals containing 13 storm periods. The cross polar cap potential inferred from AMIE inversions minus a viscous contribution described by *Boyle et al.* [1997] and included in equations (13) and (14) are plotted versus the estimated potential imposed by the solar wind ($2E_{sw}^{R}D$) in the lower panel and versus the predictions of our equation (13) in the upper panel. The solid line would imply ideal predictions. The dashed line is a least squares fit to the data. In the upper panel, the predictions agree with the measurements within or just outside the RMS deviation, but this is not true of the lower panel.

of equation (13) are equally satisfactory for the five cases not shown in the paper.

[26] In Figure 4a, the 5-min averaged values of the CPCP minus a constant viscous potential (the first term in equations (13) and (14)) are plotted versus the predictions of those equations for all 13 storms along with linear least squares fits to the data. The plots in Figure 4b are analogous to those in Figure 4a but use medians of the data in 20 kV bins. The predictions of equation (13) fall within or slightly outside the RMS scatter of the data, whereas the predictions of equation (14) overestimate them significantly at large values of $2E_{sw}^{R}D$. At the largest values of E_{sw}^{R}, although equation (13) brings the predictions much closer to the observations, it somewhat overestimates the CPCP. It is possible that during intense activity, the Pedersen conductance becomes larger than normal. Such an increase would reduce the predicted value. Alternatively, the ignored density-dependent factor may be typically larger than 1.

[27] The lower panel of Figure 4b shows that the predictions follow a linear trend when the measured CPCP is <80 kV (corresponding to a solar wind electric field ≈4 mV/m) but diverge noticeably at 100 kV and higher. These values are completely consistent with conclusions of *Russell et al.* [2001], despite the limited number of extreme cases in their data [see, e.g., *Liemohn and Ridley*, 2002]. *Russell et al.* [2001] give the critical electric field as 4 mV/m, which corresponds well to the value of 4.6 mV/m inferred from equation (11) for a nominal solar wind speed

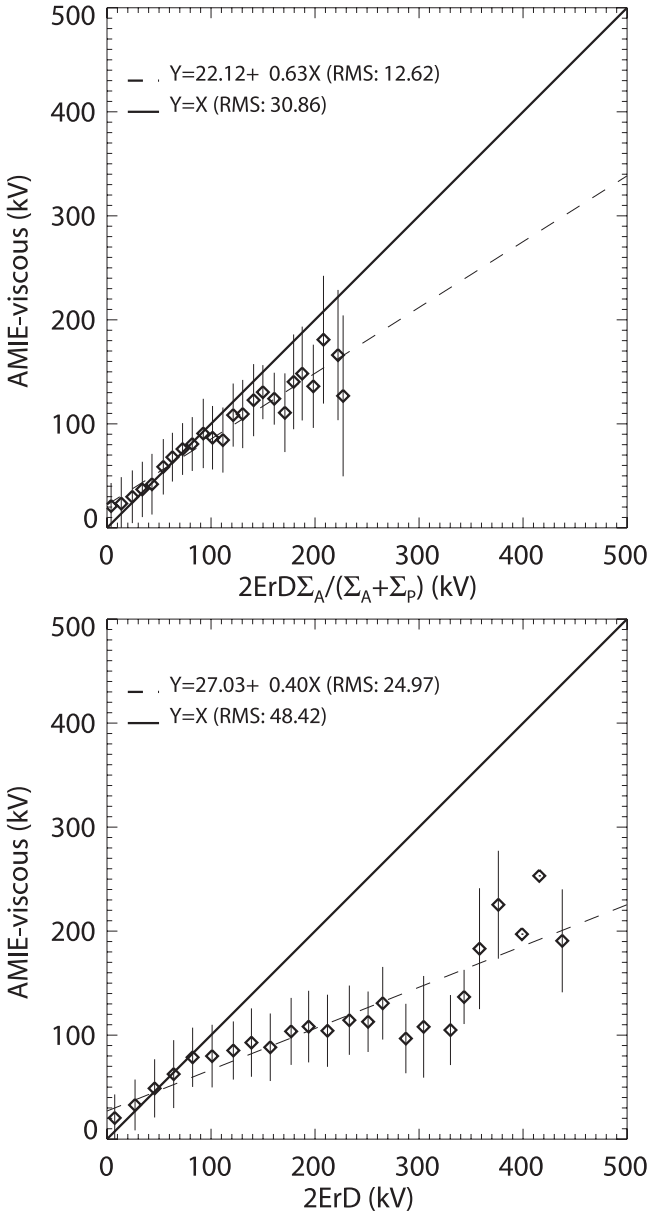

Figure 4b. As for Figure 4a but for data aggregated in 20 kV bins and fitted to the median values.

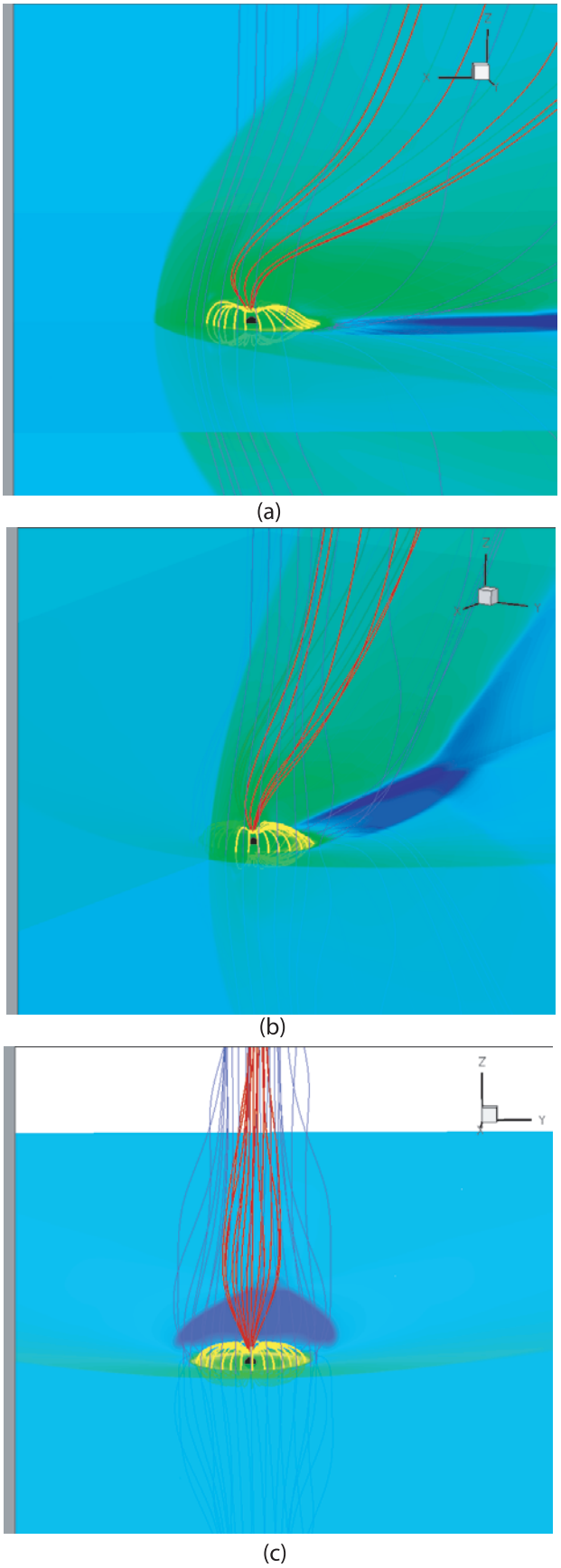

Figure 5

of 400 km/s. *Reiff et al.* [1981] estimate the critical field as ~8 nT, giving a slightly smaller critical electric field for the same assumed solar wind speed. The departure from linear predictions even for relatively small E^R_{sw} can be seen in the event plotted in Figure 3d where E^R_{sw} remains between 3 and 6 mV/m for the first 30 min, yet equation (13) improves the prediction of the CPCP relative to the linear prediction.

[28] The dashed lines in all parts of Figure 4 would be expected to go through the origin if the *Boyle et al.* [1997] expression used in equations (13) and (14) estimated the viscous contribution to the polar cap potential accurately. It appears that during storm periods the viscous response has been underestimated.

[29] The data at values of $2E^R_{sw}\,D$ greater than 100 kV but less than 350 kV in the lower panels of Figures 4a and 4b appear to trend toward an asymptotic value of the (nonviscous) polar cap potential between 100 and 150 kV. We can compare this with the limit for large v_A of equation (13)

$$\Delta V_{\max} \approx 2E^R_{sw} D\Sigma_A/\Sigma_P = 0.2\mathrm{R_E}\pi(2)^{1/6}\left(B_o\rho u^2_{sw}/\mu^2_o\right)^{1/3}\sin^2(\theta/2)\sin\lambda/\Sigma_P \quad (15)$$

where we have set $p_{sw} = \rho u^2_{sw}$. For a nominal solar wind dynamic pressure of 2 nPa and neglecting the dependence on angles, $\Delta V_{\max} \approx 150$ kV. The angular factors are always less than 1, so the saturation level is consistent with our expression.

[30] In a small fraction of the events for which $2E^R_{sw}\,D$ exceeds 350 kV, the corresponding AMIE-viscous potential exceeds 200 kV. This can be attributed to the effect of solar wind dynamic pressure in excess of nominal values. Although it is only the cube root of the dynamic pressure that enters in equation (15), peak levels in the events studied range from under 20 nPa to almost 80 nPa, introducing factors of 2.1 to 3.4 that can readily account for the higher values of the observed potential in the most extreme events. For example, the only storm in which the reconnection electric field exceeded 25 mV/m (30 March to 1 April 2001) is the only one in which the dynamic pressure of the solar wind exceeded 50 nPa, and this accounts for the data points in Figure 4b that fall far above the trend in the data.

6. Discussion

[31] In section 5, we have shown that the CPCP, including the phenomenon of saturation, is quite well represented in

Figure 5. From the simulation of *Ridley* [2007a], views of the magnetosphere illustrating aspects relevant to the arguments of this paper. The panels are viewed from different vantage points north of the equator, including (a) a location near the dusk meridian, (b) 1500 LT, and (c) near 1200 LT. Green, cyan, and blue represent velocity in the XZ and XY planes and the changes from cyan to green occur at the bow shock. Selected field lines are color coded with blue used for field lines that do not link to Earth, yellow used for closed field lines that attach at both ends to the black sphere representing Earth and red used for open field lines linking the boundary of the northern polar cap to the solar wind.

terms of the Alfvén wave analysis as expressed in equations (8) and (13), yet it is clear from Figure 4 that the scatter of predicted values is large. As noted above, there are many sources of fluctuations. For example, we have not allowed for time lags in the comparisons, but it seems reasonable that there should be some time delay in the response. There is evidence that the potential may take up to 30 min to change when the IMF is fluctuating [*Ridley et al.*, 1997] and delays of this order arise from diverse sources. For example, errors in propagating the IMF from L1 to the magnetosphere may be as large as 10–20 min [*Ridley*, 2000]. The flow slows through the magnetosheath, and even after the solar wind is linked to a polar cap flux tube, there is a further delay as the signal propagates from the magnetopause to the polar cap. Additional scatter may result from our assumption of a constant level for the viscous component of CPCP in the nonreconnecting limit. This assumption also must be, at best, an approximation. For example, at some times strong reversed convection cells [e.g., *Weimer*, 1996] can contribute significantly. (We think it likely that the polar cap flows imposed by lobe reconnection in the presence of northward IMF can also be understood in terms of Alfvén wave signals but have not addressed this feature in this paper.) Additionally, during substorms, the CPCP may increase [*Cai et al.*, 2006] through processes not directly correlated with changes in solar wind properties. For all of these reasons, we find it plausible that there is significant scatter in the plots of Figure 4, especially during periods in which the IMF is highly variable and during highly active time periods. We believe that some of these sources of scatter can be removed in a more extensive future study.

[32] Uncertainties in AMIE inversions must add to the scatter, although the consistency here demonstrated suggests that the estimates are generally quite good. As well, we have adopted a fixed value of the ionospheric conductance in the present analysis. This is clearly a significant source of error in applying the relation of equations (8) and (13) to storm-time data. It seems quite likely that during active times, Σ_P becomes larger than 10 S. Recalling that the saturated level (equation (15)) is inversely proportional to Σ_P, we note that if the assumed value of Σ_P is too small, the predicted saturation level of the CPCP will be inappropriately large. In particular, it seems reasonable that our assumption of constant Pedersen conductance may be the primary reason for the systematic overestimate of the saturation potential evident in the top panels of Figure 4. It would be of interest to investigate whether reasonable models of the dependence of the ionospheric conductance on season or activity level can improve our predictions. In a future investigation, we hope to examine the dependence of the saturation potential on each of the parameters of equation (15).

[33] In Appendix A, we have shown that the expressions used in this paper require a correction that depends weakly on the ratio of the mass density of the polar cap in the region above the current-carrying ionosphere to the mass density of the solar wind. The concept of the mass density altering the ionospheric cross polar cap potential is relatively new. Simulations done at the University of Michigan have given ambiguous results because diffusion in the model depends upon the mass density, making it difficult to distinguish numerical and physical effects. The multifluid code of *Winglee et al.* [2005] showed a clear dependence upon the mass density of the outflow, with a larger mass density producing a lower ionospheric cross polar cap potential. Our work would suggest that the opposite effect should occur.

[34] We have emphasized that our expression for the saturation potential is analogous to the form originally proposed by *Hill et al.* [1976] and is quantitatively close to that analyzed by *Siscoe et al.* [2002a], if the ionospheric conductance is taken as Siscoe's $\xi\Sigma_o$. Minor quantitative differences are accounted for in the choices of parameters relating to the length of the reconnection line. In previous studies, the saturation effect has been attributed to both internal [e.g., *Siscoe et al.*, 2002a, 2002b] and external [e.g., *Ridley*, 2005] processes. The significance of our work is that we appeal only to the physics of wave signals coupling one plasma regime to another to obtain the predicted dependence on the parameters of the system. This suggests that neither special properties of the Region 1 currents nor changes in magnetospheric geometry are fundamental to the saturation phenomenon.

[35] In Figure 5 we illustrate some of the points made in this paper using a magnetospheric simulation run for a southward magnetic field of 20 nT and $u_{sw,x} = -400$ km/s [*Ridley*, 2007a]. Orthogonal planes are colored by levels of flow speed, with the transition from cyan to green at the bow shock indicating the scale of the system. Selected solar wind field lines (blue, both ends in the solar wind), closed field lines (yellow, both ends linked to Earth) extending to just inside the magnetopause on the dayside and open field lines (red, linked at one end to the boundary of the polar cap and at the other end to the solar wind) are shown. The view is from north of the equator in all three cases. In Figure 5a the view is from close to the dusk meridian and one can immediately recognize that the solar wind end of a polar cap flux tube moves a long distance downstream as it convects across the polar cap. As they move downstream, the flux tubes experience continued deformation. This illustrates the dynamic nature of the coupling and implies that waves must continue to communicate information between the ends of the flux tubes. The view in Figure 5c from upstream in the flow illustrates clearly that in the unperturbed part of the solar wind, the cross-flow dimension of the region containing flux tubes that have connected magnetically to Earth is only a small fraction of the cross-flow dimension of the magnetopause. The bends of the field between the polar cap and the top of Figure 5 are displacements carried by the Alfvén waves that link the two regions. The wave perturbations are dominated by flows, not pressure perturbations.

[36] As Figure 5 illustrates, a wave-based analysis is required to describe how a flowing plasma is coupled to a conducting moon or magnetosphere. Relevant parts of the system are far from static over the time required for signals to link the interacting regions. If $\langle v_A \rangle$ is the average Alfvén speed along a flux tube linked to a parcel of solar wind plasma initially 30 R_E north of the polar cap, then that parcel of plasma will move more than $30R_E u_{sw}/\langle v_A \rangle$ in the antisolar direction in the time required for an Alfvén wave to travel from one end of the flux tube to the other, consistent with the structures illustrated in Figure 5, i.e., tens of R_E for reasonable estimates of $\langle v_A \rangle$. The entire flux tube undergoes

both displacement and distortion as its solar wind end is carried downstream. Circuit theory does not apply in this type of temporally varying situation, which calls for analysis in terms of wave theory. Wave analysis usually requires consideration of all the wave characteristics including the fast and slow compressional modes [*Kantrowitz and Petschek*, 1966], but the only magnetohydrodynamic wave that carries the field-aligned current that must couple into the polar cap is the Alfvén wave [see, e.g., *Kivelson*, 1995], so the other natural wave modes have been ignored in this work.

7. Summary

[37] We have presented a new framework for interpreting the phenomenon of saturation of the cross polar cap potential for large values of the solar wind electric field, proposing that the saturation arises through the increasing efficiency of wave reflection as the Alfvén speed, and hence the inverse Alfvén conductance, of the solar wind increases. The primary purpose of the data comparison presented here is to demonstrate that the predictions arising from this interpretation follow the general trend of the data during both relatively quiet and highly active times. We believe that this initial comparison is encouraging and that more refined tests of the predictions are called for. In follow-on work, we intend to allow for varying ionospheric conductance and for temporal variations of the viscous interaction and we intend to examine whether introducing temporal lags in the comparison will reduce the scatter about predicted values. We may also be able to test the contribution of the density-dependent factor, κ, that we have ignored.

[38] The authors of this work are guilty of having argued over the years that one reason to support the study of comparative magnetospheres is that such work can provide new insight into processes at work in the terrestrial magnetosphere. Thus it is a special pleasure to end this paper by noting that the interesting phenomenon that is the subject of this paper was first discussed [*Hill et al.*, 1976] in the context of the magnetospheres of the two smallest planets, Mercury and Mars (accepting that Pluto is a dwarf planet) and that our analysis was inspired by our studies of the Galilean moons of Jupiter.

Appendix A

[39] In this appendix, we relate the product of the Alfvén conductance and the electric field just above the ionosphere to their values in the solar wind. The parallel current into the ionosphere and the electric field just above the ionosphere are related by $j_{\|}(s) = \Sigma_A \nabla_\perp \cdot \mathbf{E}_\perp$ [*Neubauer*, 1980]. We seek a form that relates the parallel current into the ionosphere to parameters measured in the solar wind, the source of the Alfvénic perturbations on magnetospheric magnetic field lines linked to the polar cap. We use a curvilinear coordinate system and define the field in terms of Euler potentials (α, β) as

$$\mathbf{B} = \nabla\alpha \times \nabla\beta \tag{A1}$$

where h_α and h_β are metric coefficients that vary with $\mathbf{B}$. In describing the Alfvénic perturbation on this background field, we follow the formulation of *Singer et al.* [1981], using an orthogonal set of unit vectors:

$$\hat{\boldsymbol{\alpha}} = h_\alpha \nabla\alpha, \hat{\boldsymbol{\beta}} = h_\beta \nabla\beta, \hat{\mathbf{B}} = \nabla\alpha \times \nabla\beta / B \tag{A2}$$

The orthonormality condition implies

$$h_\alpha h_\alpha B = 1 \tag{A3}$$

The time variation of the wave is taken as $e^{-i\omega t}$, which is factored out of the equations that follow. Assume that the wave produces a displacement $\xi_\alpha(s)$, where s is distance along the background field. Neglecting thermal pressure (which is small along polar cap field lines), the α-component of the wave magnetic field, $b_\alpha(s)$, and the β-component of the wave electric field, $E_\beta(s)$, satisfy

$$b_\alpha = h_\alpha \mathbf{b} \cdot \nabla\alpha = h_\alpha \mathbf{B} \cdot (\nabla\xi_\alpha / h_\alpha) = h_\alpha B \frac{\partial}{\partial s}(\xi_\alpha / h_\alpha) \tag{A4}$$

$$E_\beta = -i\omega \xi_\alpha B \tag{A5}$$

ξ_α is governed by the wave equation [*Singer et al.*, 1981]

$$\frac{\partial^2}{\partial s^2}\left(\frac{\xi_\alpha}{h_\alpha}\right) + \frac{\partial}{\partial s}\left(\ln\left(h_\alpha^2 B\right)\right)\frac{\partial}{\partial s}\left(\frac{\xi_\alpha}{h_\alpha}\right) + \frac{\mu_o \rho \omega^2}{B^2}\left(\frac{\xi_\alpha}{h_\alpha}\right) = 0 \tag{A6}$$

Above the ionosphere, one can assume that the background field and plasma properties vary on a spatial scale large compared with the wavelength of the Alfvénic perturbations linking the solar wind to the ionosphere. For these conditions, the WKB method can be used to approximate a solution to equation (A6). We set

$$\xi_\alpha(s)/h_\alpha = Ce^{i\varphi(s)} \tag{A7}$$

where C is independent of s but both C and φ may depend on α and β. Then

$$i\varphi'' + \omega^2/\mathrm{v}_A^2 - (\varphi')^2 + i\varphi' \partial\left[\ln\left(h_\alpha/h_\beta\right)\right]/\partial s = 0 \tag{A8}$$

In the limit of a uniform field and plasma background, the derivative of $\ln(h_\alpha/h_\beta)$ vanishes and the second derivative of the phase, φ, vanishes, so neither of last two terms is finite. For weakly varying background properties, one assumes that these terms are smaller than the leading terms. In this case we can expand φ to second order as $\varphi = \varphi_1 + \varphi_2$ where φ_1 satisfies

$$(\varphi_1')^2 = \omega^2/\mathrm{v}_A^2 \text{ or } \varphi_1(s) = \pm\int_{s_o}^{s} ds'\omega/\mathrm{v}_\mathrm{A}(s') \tag{A9}$$

and φ_2 satisfies

$$i\varphi_1'' - 2\varphi_1'\varphi_2' + i\varphi_1' \partial\left[\ln\left(h_\alpha/h_\beta\right)\right]/\partial s = 0 \tag{A10}$$

or

$$\varphi_2(s) = i\ln\left(\frac{h_\alpha}{h_\beta}\frac{h_{\beta o}}{h_{\alpha o}}\frac{\mathrm{v}_A(s_o)}{\mathrm{v}_A(s)}\right)^{1/2} \tag{A11}$$

where s_o is taken to be at the source of the flux tube in the solar wind. Finally,

$$\xi_\alpha(s)/h_\alpha = C\left(\frac{h_\beta}{h_\alpha}\frac{h_{\alpha o}}{h_{\beta o}}\frac{\mathrm{v}_A(s)}{\mathrm{v}_A(s_o)}\right)^{1/2}\exp\left[i\int_{s_o}^{s} ds'\omega/\mathrm{v}_A(s')\right] \tag{A12}$$

Correspondingly,

$$E_\beta(s) = -i\omega CB(s)h_\alpha\left(\frac{h_{\alpha o}}{h_{\beta o}}\frac{h_\beta}{h_\alpha}\frac{\mathrm{v}_A(s)}{\mathrm{v}_A(s_o)}\right)^{1/2}\exp\left[i\int_{s_o}^{s} ds'\omega/\mathrm{v}_A(s')\right] \tag{A13}$$

$$b_\alpha(s) = Ch_\alpha B(s)\frac{\partial}{\partial s} \times\left[\left(\frac{h_{\alpha o}}{h_{\beta o}}\frac{h_\beta}{h_\alpha}\frac{\mathrm{v}_A(s)}{\mathrm{v}_A(s_o)}\right)^{1/2}\exp\left[i\int_{s_o}^{s} ds'\omega/\mathrm{v}_A(s')\right]\right] \tag{A14}$$

From these solutions, one can show that the Poynting vector (**S**) is proportional to **B**(s), and thus that the integral power transmitted along a flux tube (whose cross section is proportional to $B(s)^{-1}$) is independent of s. By definition

$$\mathbf{S} = -(4\mu_o)^{-1}\left(\mathbf{E}\times\mathbf{b}^* + \mathbf{E}^*\times\mathbf{b}^*\right)$$

From equations (A4) and (A5) and the WKB assumption, it follows that $b_\alpha\,(s) = E_\beta/\mathrm{v}_A\,(s)$ and that

$$\begin{aligned}\mathbf{S} &= h_\alpha h_\beta(\nabla\beta\times\nabla\alpha)|E_\beta(s)|^2/2\mu_o\mathrm{v}_A(s)\\ &= \mathbf{B}(s)h_\alpha h_\beta|E_\beta(s)|^2/2\mu_o\mathrm{v}_A(s)\end{aligned}$$

Here $\mathbf{B}(s)h_\alpha h_\beta$ is a unit vector along the background field so

$$\mathbf{S} = \hat{\mathbf{B}}|E_\beta(s)|^2/2\mu_o\mathrm{v}_A(s) \tag{A15}$$

and with $|E_\beta(s)|^2/\mathrm{v}_A(s) = \frac{h_{\alpha o}}{h_{\beta o}}\frac{\omega^2C^2B(s)}{\mathrm{v}_A(s_o)}$ we find

$$\mathbf{S} = \frac{\mathbf{B}(s)}{2\mu_o}\frac{h_{\alpha o}}{h_{\beta o}}\frac{\omega^2C^2}{\mathrm{v}_A(s_o)} \text{ and } \mathbf{S}_o = \frac{\mathbf{B}_o(s)}{2\mu_o}\frac{h_{\alpha o}}{h_{\beta o}}\frac{\omega^2C^2}{\mathrm{v}_A(s_o)}$$

From this it follows that the integral wave power in the flux tube satisfies

$$\int \mathbf{S}\cdot\mathbf{dA} = \int \mathbf{S}_o\cdot\mathbf{dA}_o \tag{A16}$$

where the integrals are taken over the cross section of the flux tube.

[40] We seek to understand how an Alfvénic signal launched into polar cap field lines is reflected from the ionosphere. The analysis is based on continuity of current and, in a uniform field leads to the identity $j_\parallel = \Sigma_A\nabla\cdot\mathbf{E}_\perp$ (explicit in the work of *Neubauer* [1980] and implicit in the work of *Mallinckrodt and Carlson* [1978]) where neither Σ_A nor $\mathbf{E}_\perp$ vary along the background field. Here we ask how this relation is modified when both the field and the density vary with s. We seek to understand how the parallel current just above the ionosphere relates to the electric field and the Alfvén speed at the source of the signal in the solar wind. We will find no dependence on the change of field magnitude between the source and the ionosphere, but that the change of density between the solar wind and the ionospheric end of the flux tube requires a correction factor of order 1.

[41] The derivation requires use of the dispersion relation for the Alfvénic signal. From Faraday's law

$$i\omega b_\alpha = -\frac{1}{h_\beta}\frac{\partial}{\partial s}\left(h_\beta E_\beta\right) \tag{A17}$$

The momentum equation combined with Ampere's law gives

$$j_\beta = -i\omega\rho E_\beta/B^2 = -i\omega E_\beta/\mu_o\mathrm{v}_A^2 = \frac{1}{\mu_o h_\alpha}\frac{\partial(h_\alpha b_\alpha)}{\partial s} \tag{A18}$$

and thus

$$\omega^2 b_\alpha = \text{`} - \frac{1}{h_\beta}\frac{\partial}{\partial s}\left(\frac{\mathrm{v}_A^2 h_\beta}{h_\alpha}\frac{\partial(h_\alpha b_\alpha)}{\partial s}\right) \tag{A19}$$

We assumed that the background properties vary on a scale long compare with the wavelength in the direction along the field (the WKB approximation), so the derivatives in equation (A19) apply only to b_α. Using a local wave number, $k(s)$, set $\partial b_\alpha/\partial s \approx ik(s)b_\alpha$. It then follows that $\omega^2\ b_\alpha\ (s) \approx k(s)^2\mathrm{v}_A^2(s)b_\alpha\ (s)$, and correspondingly $\omega \approx \pm\ k(s)\mathrm{v}_A\ (s)$.

[42] The parallel current satisfies

$$\begin{aligned}j_\parallel &= \hat{\mathbf{B}}\cdot(\nabla\times\mathbf{b})/\mu_o = \hat{\mathbf{B}}\cdot(\nabla\times b_\alpha h_\alpha\nabla\alpha)/\mu_o\\ &= -\hat{\mathbf{B}}\cdot(\nabla\alpha\times\nabla b_\alpha h_\alpha)/\mu_o = -\left(\hat{\mathbf{B}}\times\nabla\alpha\right)\cdot\nabla b_\alpha h_\alpha)/\mu_o\\ &= -\left[\left(\hat{\mathbf{B}}\times\hat{\boldsymbol{\alpha}}\right)\cdot\nabla b_\alpha h_\alpha)\right]/\mu_o h_\alpha = -\frac{1}{\mu_o h_\alpha h_\beta}\nabla_\beta(b_\alpha h_\alpha)\end{aligned} \tag{A20}$$

Inserting equation (A17), one finds

$$j_\parallel = \frac{1}{i\omega\mu_o h_\alpha h_\beta}\nabla_\beta\left(\frac{h_\alpha}{h_\beta}\frac{\partial}{\partial s}h_\beta E_\beta\right) \approx \frac{k(s)}{\omega\mu_o h_\alpha h_\beta}\nabla_\beta h_\alpha E_\beta(s)$$

again using the WKB assumption. Finally

$$j_\parallel \approx \frac{1}{\mu_o\mathrm{v}_A(s)}\nabla_\perp\cdot E_\perp(s) \tag{A21}$$

From the fact that the integral of the Poynting vector over flux tube area is constant, it follows that $E_\beta(s) \approx [B(s)\mathrm{v}_A(s)/B(s_o)\mathrm{v}_A\ (s_o)]^{1/2}E_\beta(s_o)$, or

$$E_\beta(s) = \left[\frac{\rho(s_o)}{\rho(s)}\right]^{1/4}\left[\frac{B(s)}{B(s_o)}\right]E_\beta(s_o) \tag{A22}$$

This form reflects the fact that as the signal approaches the ionosphere the electric field increases because the equipo-

tential field lines converge (an increase proportional to $B^{1/2}$) and also changes because the propagation speed changes (contributing a factor proportional to $v_A^{1/2}$). Inserting equation (A22) into (A21), we obtain

$$j_{\parallel}(s) \approx [\rho(s)/\rho(s_o)]^{1/4}\Sigma_A(s_o)\nabla_{\perp}\cdot\mathbf{E}_{\perp}(s_o) \qquad \text{(A23)}$$

This is the form that we are seeking. It shows that the parallel current into the ionosphere can be calculated from the Alfvén conductance in the solar wind with a correction factor $[\rho(s)/\rho_{SW}]^{1/4}$ that we will next argue is of order 1.

[43] We do not have extensive measurements of the plasma density in the polar cap in the region just above the current-carrying region of the ionosphere where the WKB approximation breaks down. It is known to be variable with both activity and season. However, the fourth root in equation (A23) implies that the correction factor relevant to our work is not extremely sensitive to variations. *Chugunin et al.* [2002] give quiet time densities of order 1 cm^{-3} at $\sim$3 R_E, which is a bit higher than relavant to this discussion. *Huddleston et al.* [2005] indicate that the average polar wind H^+ density (including both quiet and active times) at 5000 km altitude is 34 cm^{-3}, noting that densities roughly double during active times. *Laasko et al.* [2002] report densities typically less than 50 cm^{-3} over the low-altitude polar cap (near 0.9 R_E), with typical values between 10 and 100 cm^{-3}. For nominal solar wind density of $\sim$10 cm^{-3}, the correction factors would range from 1 to 1.78, and for the higher solar wind densities (say $\sim$50 cm^{-3}) typical of the storm intervals for which we seek saturation levels, the range would be from 0.66 to 1.2. Thus, the expected correction factor is of order 1 and ignoring it introduces an uncertainty of order tens of percent.

[44] **Acknowledgments.** MGK acknowledges support from the National Science Foundation under grant ATM02–05958 and from NASA under grant NNG06GG67G. She appreciates having been given the opportunity to pursue this work during a visit to the Department of Atmospheric, Oceanic and Space Sciences at the University of Michigan. AJR acknowledges support from NSF grants ATM-0417839 and ATM-0325332 and NASA grant NNG04GK18G. Both authors appreciate discussions with K.C. Hansen and R. J. Strangeway. MK appreciated the helpful discussion of the WKB approximation for wave propagation in a nonuniform medium on the Website of Richard Fitzpatrick (University of Texas at Austin). We are grateful to one of the reviewers whose thoughtful criticism enabled us to make essential changes to the paper. UCLA Institute of Geophysics and Planetary Physics Publication 6339.

[45] Zuyin Pu thanks the reviewers for their assistance in evaluating this paper.

References

Bekerat, H. A., R. W. Schunk, L. Scherliess, and A. Ridley (2005), Comparison of satellite ion drift velocities with AMIE deduced convection patterns, *J. Atmos. Sol. Terr. Phys.*, *67*, 1463, doi:10.1016/j.jastp.2005.08.013.

Boyle, C. B., P. H. Reiff, and M. R. Hairston (1997), Empirical polar cap potentials, *J. Geophys. Res.*, *102*, 111, doi:10.1029/96JA01742.

Cai, X., C. R. Clauer, and A. J. Ridley (2006), Statistical analysis of ionospheric potential patterns for isolated substorms and sawtooth events, *Ann. Geophys.*, *24*, 1977.

Chugunin, D. V., L. V. Zinin, Y. I. Galperin, N. Dubouloz, and M. Bouhram (2002), Polar wind observations on the nightside of the polar cap at Altitudes of 2–3 R_E: Results of the INTERBALL-2 satellite, *Ann. Geophys.*, *40*, 416.

Friis-Christensen, E., Y. Kamide, A. Richmond, and S. Matsushita (1985), Interplanetary magnetic field control of high-latitude electric fields and currents determined from Greenland magnetometer chain, *J. Geophys. Res.*, *90*, 1325, doi:10.1029/JA090iA02p01325.

Hairston, M. R., T. W. Hill, and R. A. Heelis (2003), Observed saturation of the ionospheric polar cap potential during the 31 March 2001 storm, *Geophys. Res. Lett.*, *30*(6), 1325, doi:10.1029/2002GL015894.

Hairston, M. R., K. A. Drake, and R. Skoug (2005), Saturation of the ionospheric polar cap potential during the October–November 2003 superstorms, *J. Geophys. Res.*, *110*, A09S26, doi:10.1029/2004JA010864.

Hill, T. W. (1984), Magnetic coupling between the solar wind and magnetosphere: Regulated by ionospheric conductance?, *Eos Trans. AGU*, *65*, 1047.

Hill, T. W., A. J. Dessler, and R. A. Wolf (1976), Mercury and Mars: The role of ionospheric conductivity in the acceleration of magnetospheric particles, *Geophys. Res. Lett.*, *3*, 429, doi:10.1029/GL003i008p00429.

Huddleston, M. M., C. R. Chappell, D. C. Delcourt, T. E. Moore, and M. O. Chandler (2005), An examination of the process and magnitude of ionospheric plasma supply to the magnetosphere, *J. Geophys. Res.*, *110*, A12202, doi:10.1029/2004JA010401.

Kan, J., and L. Lee (1979), Energy coupling function and solar wind magnetosphere dynamo, *Geophys. Res. Lett.*, *6*, 577, doi:10.1029/GL006i007p00577.

Kantrowitz, A. R., and H. E. Petschek (1966), MHD characteristics and shock waves, in *Plasma Physics in Theory and Application*, edited by W. B. Kunkel, McGraw-Hill, New York.

Kihn, E. A., et al. (2006), A statistical comparison of the AMIE derived and DMSP-SSIES observed high-latitude ionospheric electric field, *J. Geophys. Res.*, *111*, A08303, doi:10.1029/2005JA011310.

Kivelson, M. G. (1995), Pulsations and magnetohydrodynamic waves, in *Introduction to Space Physics*, edited by M. G. Kivelson and C. T. Russell, pp. 330–355, Cambridge Univ. Press, New York.

Kivelson, M. G., F. Bagenal, W. S. Kurth, F. M. Neubauer, C. Paranicas, and J. Saur (2004), Magnetospheric interactions with satellites, in *Jupiter: The Planet, Satellites and Magnetosphere*, edited by F. Bagenal, T. Dowling, and W. McKinnon, chap. 21, 513 pp., Cambridge Univ. Press, New York.

Laasko, H., R. Pfaff, and P. Janhunen (2002), Polar observations of electron density distributions in the Earth's magnetosphere. 2. Density profiles, *Ann. Geophys.*, *20*, 1725.

Liemohn, M. W., and A. J. Ridley (2002), Comment on "Nonlinear response of the polar ionosphere to large values of the interplanetary electric field" by C. T. Russell et al., *J. Geophys. Res.*, *107*(A12), 1460, doi:10.1029/2002JA009440.

Liemohn, M. W., J. U. Kozyra, T. H. Zurbuchen, A. J. Ridley, G. Lu, M. Hairston, and D. Weimer (2002), Consequences of a saturated convection electric field on the ring current, *Geophys. Res. Lett.*, *29*(9), 1348, doi:10.1029/2001GL014270.

Mallinckrodt, A. J., and C. W. Carlson (1978), Relations between transverse electric field and field-aligned currents, *J. Geophys. Res.*, *83*, 1426, doi:10.1029/JA083iA04p01426.

Merkine, V. G., K. Papadopoulos, G. Milikh, A. S. Sharma, X. Shao, J. Lyon, and C. Goodrich (2003), Cross polar cap potential: MHD modeling, *Geophys. Res. Lett.*, *30*(23), 2180, doi:10.1029/2003GL017903.

Neubauer, F. M. (1980), Nonlinear standing Alfvén wave current system at Io: Theory, *J. Geophys. Res.*, *85*, 1171, doi:10.1029/JA085iA03p01171.

Papitashvili, V., B. Belov, D. Faermark, Y. Feldstein, S. Golyshev, L. Gromova, and A. Levitin (1994), Electric potential patterns in the northern and southern polar regions parameterized by the interplanetary magnetic field, *J. Geophys. Res.*, *99*, 13,251, doi:10.1029/94JA00822.

Parker, E. (2007), *Conversations on Electric and Magnetic Fields in the Cosmos*, Princeton Univ. Press, Princeton, N. J.

Reiff, P., R. Spiro, and T. Hill (1981), Dependence of polar cap potential on interplanetary parameters, *J. Geophys. Res.*, *86*, 7639, doi:10.1029/JA086iA09p07639.

Richardson, I. G., et al. (2006), Major geomagnetic storms (Dst <= −100 nT) generated by corotating interaction regions, *J. Geophys. Res.*, *111*, A07S09, doi:10.1029/2005JA011476.

Richmond, A., and Y. Kamide (1988), Mapping electrodynamic features of the high-latitude ionosphere from localized observations: Technique, *J. Geophys. Res.*, *93*, 5741, doi:10.1029/JA093iA06p05741.

Ridley, A. J. (2000), Estimation of the uncertainty in timing the relationship between magnetospheric and solar wind processes, *J. Atmos. Sol. Terr. Phys.*, *62*, 757, doi:10.1016/S1364-6826(00)00057-2.

Ridley, A. J. (2005), A new formulation for the ionospheric cross polar cap potential including saturation effects, *Ann. Geophys.*, *23*, 3533.

Ridley, A. J. (2007a), Alfvén wings at Earth's magnetosphere under strong interplanetary magnetic field, *Ann. Geophys.*, *25*, 533.

Ridley, A. J. (2007b), Effects of seasonal changes in the ionospheric conductance on magnetospheric field-aligned currents, *Geophys. Res. Lett.*, *34*, L05101, doi:10.1029/2006GL028444.

Ridley, A., and E. Kihn (2004), Polar cap index comparisons with AMIE cross polar cap potential, electric field, and polar cap area, *Geophys. Res. Lett.*, *31*, L07801, doi:10.1029/2003GL019113.

Ridley, A. J., G. Lu, C. R. Clauer, and V. O. Papitashvili (1997), Ionospheric convection during nonsteady interplanetary magnetic field conditions, *J. Geophys. Res.*, *102*, 14,563, doi:10.1029/97JA00940.

Ridley, A., G. Crowley, and C. Freitas (2000), A empirical model of the ionospheric electric potential, *Geophys. Res. Lett.*, *27*, 3675, doi:10.1029/1999GL011161.

Russell, C. T., J. G. Luhmann, and G. Lu (2001), Nonlinear response of the polar ionosphere to large values of the interplanetary electric field, *J. Geophys. Res.*, *106*, 18,495, doi:10.1029/2001JA900053.

Shepherd, S. G. (2007), Polar cap potential saturation: Observations, theory, and modeling, *J. Atmos. Sol. Terr. Phys.*, *69*, 234, doi:10.1016/j.jastp.2006.07.022.

Shepherd, S. G., R. A. Greenwald, and J. M. Ruohoniemi (2002), Cross polar cap potentials measured with Super Dual Auroral Radar Network during quasi-steady solar wind and interplanetary magnetic field conditions, *J. Geophys. Res.*, *107*(A7), 1094, doi:10.1029/2001JA000152.

Singer, H. J., D. J. Southwood, R. J. Walker, and M. G. Kivelson (1981), Alfven wave resonances in a realistic magnetospheric field geometry, *J. Geophys. Res.*, *86*, 4589, doi:10.1029/JA086iA06p04589.

Siscoe, G. L., G. M. Erickson, B. U. Ö. Sonnerup, N. C. Maynard, J. A. Schoendorf, K. D. Siebert, D. R. Weimer, W. W. White, and G. R. Wilson (2002a), Hill model of transpolar potential saturation: Comparisons with MHD simulations, *J. Geophys. Res.*, *107*(A6), 1075, doi:10.1029/2001JA000109.

Siscoe, G. L., N. U. Crooker, and K. D. Siebert (2002b), Transpolar potential saturation: Roles of region 1 current system and solar wind ram pressure, *J. Geophys. Res.*, *107*(A10), 1321, doi:10.1029/2001JA009176.

Sonnerup, B. (1974), Magnetopause reconnection rate, *J. Geophys. Res.*, *79*, 1546, doi:10.1029/JA079i010p01546.

Southwood, D. J., M. G. Kivelson, R. J. Walker, and J. A. Slavin (1980), Io and its plasma environment, *J. Geophys. Res.*, *85*, 5959, doi:10.1029/JA085iA11p05959.

Weimer, D. R. (1996), A flexible, IMF dependent model of high-latitude electric potential having "space weather" applications, *Geophys. Res. Lett.*, *23*, 2549, doi:10.1029/96GL02255.

Weimer, D., L. Reinleitner, J. Kan, L. Zhu, and S.-I. Akasofu (1990), Saturation of the auroral electrojet current and the polar cap potential, *J. Geophys. Res.*, *95*, 18,981, doi:10.1029/JA095iA11p18981.

Winglee, R. M., W. Lewis, and G. Lu (2005), Mapping of the heavy ion outflows as seen by the IMAGE and multifluid global modeling for the 17 April 2002 storm, *J. Geophys. Res.*, *110*, A12S24, doi:10.1029/2004JA010909.

Wright, A. W. (1996), Transfer of magnetosheath momentum and energy to the ionosphere along open field lines, *J. Geophys. Res.*, *101*, 13,169, doi:10.1029/96JA00541.

M. G. Kivelson, Institute of Geophysics and Planetary Physics, University of California, Los Angeles, 405 Hilgard Avenue, Los Angeles, CA 90095-1567, USA. (mikivelson@igpp.ucla.edu)

A. J. Ridley, Department of Atmospheres, Oceans, and Space Sciences, University of Michigan, Ann Arbor, MI 48109-2143, USA.